NASA CONTRACTOR REPORT

NASA CR-211

EXPERIMENTAL INVESTIGATION OF THE OPACITY OF SMALL PARTICLES

by P. J. Marteney

Prepared under Contract No. NASw-847 *by*
UNITED AIRCRAFT CORPORATION
East Hartford, Conn.
for

NATIONAL AERONAUTICS AND SPACE ADMINISTRATION • WASHINGTON, D. C. • APRIL 1965

NASA CR-211

EXPERIMENTAL INVESTIGATION OF THE OPACITY OF SMALL PARTICLES

By P. J. Marteney

Prepared under Contract No. NASw-847 by
UNITED AIRCRAFT CORPORATION
East Hartford, Conn.

for

NATIONAL AERONAUTICS AND SPACE ADMINISTRATION

For sale by the Office of Technical Services, Department of Commerce,
Washington, D.C. 20230 -- Price $3.00

Experimental Investigation of the

Opacity of Small Particles

TABLE OF CONTENTS

Experimental Investigation of the Opacity of Small Particles

SUMMARY

An experimental investigation was conducted to develop a technique for producing dispersions of submicron-radius solid particles in a carrier gas and to determine the optical parameters of these particles as a function of the wave length of electromagnetic radiation incident upon the particles. A dispersion system was devised which permitted (a) mixing of measured amounts of agglomerated submicron particles with metered quantities of preselected carrier gases, (b) application of de-agglomerative aerodynamic shear forces in a restrictive flow passage (nozzle) through which the carrier gas-particle mixture was passed, and (c) measurement of the extinction and scattering characteristics of the de-agglomerated particles downstream of the nozzle. Tests were conducted with carbon and tungsten particles having nominal radii of 0.0045 and 0.01 microns, respectively, as specified by the manufacturer. Helium and nitrogen were used as carrier gases.

The application of aerodynamic shear forces in the tests resulted in an increase in the extinction parameter for carbon particles from approximately 10,000 cm^2/gm to 58,000 cm^2/gm and for tungsten particles from approximately 2000 cm^2/gm to 8000 cm^2/gm. These increases in extinction parameter are believed to be caused by a reduction in the size of particle agglomerates since, for the sizes of agglomerates encountered in the test program, a reduction in the average agglomerate size should theoretically result in an increase in extinction parameter. Particle photographs qualitatively indicated that the sizes of particle agglomerates were reduced by the application of aerodynamic shear. The maximum theoretical extinction parameters for carbon and tungsten particles at a wavelength of 0.4 microns are 68,000 cm^2/gm and 20,000 cm^2/gm, and occur for particles having radii of 0.1 and 0.05 microns, respectively. The differences between theoretical and experimental maximum extinction parameters can be explained by the presence of a range of particle agglomerate sizes in the experimental program and by the theoretical variation of extinction parameter with particle size.

CONCLUSIONS

1. The application of aerodynamic shear to a particle-gas stream can result in a decrease in the size of particle agglomerates present in the stream and correspondingly will result in an increase in the opacity of the particles if the opacity associated with the original size of the particle agglomerates is less than the opacity associated with the smaller agglomerate sizes.

2. The difference between theoretical and measured maximum extinction coefficients in a de-agglomerated particle-gas stream is due at least in part to the presence in the de-agglomerated stream of particle agglomerates having sizes both smaller and larger than the particle agglomerate size which theoretically results in the maximum extinction parameter. The test results indicated that the ratio of maximum measured to maximum theoretical extinction coefficient was 0.85 and 0.40 for carbon and tungsten particles, respectively.

INTRODUCTION

The addition of small amounts of an opaque seed to the hydrogen propellant of a gaseous core nuclear rocket (Refs. 1 and 2) has been proposed to ensure adequate radiant energy absorption by the propellant and to prevent excessive radiant heat transfer to the confining chamber walls. It is necessary to add seeding materials to hydrogen because hydrogen is effectively transparent to electromagnetic radiation at low temperatures; i.e., at temperatures below approximately 5000-6000 K (Refs. 3 and 4). Seed materials of possible interest include low-ionization-potential metal vapors, polyatomic gases, and small-size liquid or solid particles. The small-size particles are potentially the most useful seed materials in view of their nearly continuous absorption over a wide range of wavelengths in contrast to the discrete spectral absorption of the low-ionization-potential metals and the polyatomic gases (Ref. 5).

Small-size particles should be effective absorbers of thermal radiation for temperatures ranging from the propellant injection temperature up to the temperature at which the particles either vaporize or react chemically with the propellant. Analytical studies (Ref. 6) have indicated that a number of pure metals are well suited for use as propellant seed materials because they do not react appreciably with hydrogen and because they possess high melting- and boiling-point temperatures. One of these materials is tungsten, whose melting- and boiling-point temperatures are 3650 and 5645 K, respectively. Theoretical calculations of the absorption and extinction parameters of 15 materials (Ref. 7) indicate, however, that the opacity afforded by tungsten is only about one-third that of carbon. The theoretical maximum extinction parameter for carbon at a wavelength of 0.4 microns is approximately 68,000 cm^2/gm in contrast to a value of 20,000 cm^2/gm for tungsten. However, carbon is probably not a feasible seed material because it reacts with hydrogen and in addition sublimes at about 4200 K, but it is obvious that several criteria must be observed in selecting the most effective seed material.

Measurements of the extinction characteristics of small particles are presented in Refs. 5, 8 and 9. The extinction parameters measured in the tests reported in Ref. 8, which were conducted with the particles suspended in water, yielded extinction parameters for graphite particles from 6000 to 14,000 cm^2/gm. Photographs of particles presented in Ref. 8 indicated that these low values of extinction parameter relative to theory could be due to particle agglomeration. Preliminary measurements reported in Ref. 5 of extinction parameters of particles dispersed in a gas stream indicated that the extinction parameter could be increased due to aerodynamic shear created by passage of the particle-gas stream through a small nozzle. Measurements which are reported in Ref. 9 and which were made in tests in which carbon particles were suspended in an air stream passing adjacent to an arc discharge indicated a value of extinction parameter of 22,000 cm^2/gm. Since the measured extinction parameters are lower than theory, and since the theoretical extinction parameter decreases with an increase in particle size, it appeared possible

to increase the measured extinction parameter by particle de-agglomeration. However, experience relating to the production of dispersions of particles in the submicron size range is extremely limited. Submicron particles exhibit such a strong tendency toward agglomeration that they are rarely found as single entities, and the aggregates which are formed possess high tensile strengths (Refs. 10 and 11).

The difficulty in separating submicron particles may be contrasted to the ease of separation of particles having radii of the order of centimeters or larger, which do not usually agglomerate. The common methods of separation for these larger size particles include screening and air or water sedimentation. However, these methods are not applicable to the separation of submicron particles since they do not furnish the means for adding enough energy to rupture the strong bonds maintaining the agglomerates. Hence, the primary objective of the study reported herein was to devise an effective means of producing dispersions of submicron particles in a gas, and then to measure the optical properties of these dispersed submicron particles as a function of the wavelength of the radiation incident upon the particles. Carbon and tungsten were selected as the primary materials to be investigated.

THEORETICAL EXTINCTION AND SCATTERING BY SMALL-DIAMETER PARTICLES

The theoretical extinction, absorption and scattering characteristics of small-diameter particles are described by the Mie equations. As part of the overall investigations performed under this contract, the Mie equations were programmed for solution on the IBM 7090 machine. Results of calculations made using this machine program for 15 materials are described in detail in Ref. 7.

Typical results from Ref. 7 for carbon and tungsten particles are shown in Figs. 1 and 2, respectively. For each of these figures the effect of particle radius on the extinction and absorption parameters is shown for several wavelengths of incident light. The maximum extinction parameter calculated for carbon at a wavelength of 0.4 microns is 68,000 cm^2/gm, and is observed to occur for a particle radius of 0.1 microns. The maximum extinction parameter calculated for tungsten at a wavelength of 0.4 microns is 20,000 cm^2/gm and occurs at a particle radius of 0.05 microns. As is evident in Figs. 1 and 2, the maximum extinction parameters for wavelengths of light greater than 0.4 microns also occur for particles having radii much smaller than one micron, although the particle radius for maximum extinction increases as the incident light wavelength increases.

PRODUCTION OF SMALL-DIAMETER PARTICLES

Standard Methods of Production

Particles having diameters of the order of several hundred microns can be produced by mechanical means (such as crushing or grinding of large units or by agglomeration of smaller primary particles), whereas particles having radii of the order of one micron or less are nearly exclusively formed by controlled aggregation following chemical reaction. (The arduous process of producing submicron particles by liquid-phase grinding is described in Ref. 12; unsatisfactory dry-milling is also described in Ref. 12.) To illustrate, submicron-size carbon particles are formed in oxygen-lean flames; powders of metal oxides such as silica or alumina are formed during combustion of the metal; and powders of metals such as tungsten, nickel, and molybdenum, are produced by hydrogen reduction of a volatile halide. In all the above cases, the conditions of reaction (e.g., flow rate, temperature, pressure and stoichiometry) determine the sizes of particles produced, and particle diameters as small as 0.0025 microns (10 to 20 atomic diameters) have been obtained.

The rate of agglomeration of these submicron particles is determined by the local balance of separative and cohesive forces present following formation. Dilution, rapid flow and high reacting temperatures inhibit agglomeration; high particle concentration, slow flow and lower temperatures promote growth of large particles (Ref. 13).

The forces responsible for holding agglomerated particles together may be grouped into two types (Ref. 10): liquid-bridge forces resulting from the formation of a capillary junction between liquids absorbed on the surfaces of particles, and electrostatic attractions (such as van der Waals forces), which may arise from charged-particle interactions for particles having dry surfaces. The liquid-bridge forces are considerably stronger than the van der Waals forces; however, in the absence of surface adherents, the magnitude of the van der Waals forces per unit area can be large if the particle radii are of the order of 1 micron or less.

De-Agglomeration Methods

The only means of accomplishing de-agglomeration of submicron particles is to add sufficient energy to individual particles to counter the cohesive forces between the particles. Such energy addition may be achieved by ultrasonic agitation (Ref. 8) or by application of wetting agents in liquid systems (Ref. 14) or by particle-wall impact in gas streams (Ref. 15). The system developed for use in the present investigations is unique in that substantial aerodynamic shear forces were applied to a particle-laden gas stream which had previously been subjected to impact forces.

EXPERIMENTAL APPARATUS AND TECHNIQUES

The experimental apparatus employed in this investigation is illustrated schematically in Figs. 3 through 6. The apparatus was designed to (a) produce a particle-gas stream of known composition, (b) allow the application of de-agglomerative forces to the particle-gas stream through the use of aerodynamic shear, (c) permit measurement of the optical properties of de-agglomerated particles as a function of experimental conditions, and (d) permit sampling of the stream so that the size of particles could be estimated. The apparatus consisted of a dispersion system (in which large agglomerates of particles were mixed with a carrier gas and then acted upon by aerodynamic shear forces which caused rupture of the agglomerates) and an optical system used to measure the extinction and scattering parameters. These are discussed individually below.

Dispersion System

A particle-gas stream of known composition was produced by passing metered quantities of helium or nitrogen gases through a Wright Dust Feed Mechanism (Ref. 15), manufactured by L. Adams, Ltd., London, England. In this mechanism, dust is stored within a variable-volume cylinder. One end-wall and the peripheral wall of the cylinder rotate and advance along a lead screw toward the fixed end of the cylinder. A scraper blade is mounted on the fixed end of the cylinder. The carrier gas is injected under the scraper blade and carries away all of the powder removed by the blade. In the tests described in the present report, all of the carrier gas was passed through the dust feed mechanism (i.e., no gas was added downstream of the dust feed mechanism).

The Wright Dust Feed Mechanism also incorporates a flat impact plate at which the particle-gas stream is directed through a small jet tube having a diameter of 0.052 in. The rebounding particles and carrier gas were then passed from the feed mechanism into a reservoir (Fig. 4) which contained the dispersing nozzle assemblies. It was the intended purpose of the dispersing nozzle to reduce the size of particles passing through it by the application of shear forces due to a steep velocity gradient arising from a combination of near-sonic flow in the nozzle and the use of small-diameter passages. Typical dispersing nozzle assemblies are illustrated in Figs. 5 and 6. Nozzle passages employed in these tests were 0.020 in. in diameter. During preliminary tests, larger diameters of passages (0.040 and 0.080 in.) were found to have little effect in particle size reduction, as evidenced by low, nearly constant values of the mass extinction parameter (Ref. 5). A smaller passage (0.014 in.) tended to exhibit plugging due to the presence of large agglomerates despite preliminary seiving of the samples. Passage lengths varied from 0.25 to 1.25 in.

Optical System

The optical system, shown schematically in Fig. 3, included an ac-operated BH-6 high-pressure mercury lamp and a 1P21 photomultiplier tube detector, operated at a potential of 800 v. dc. The phototube was connected to a type "E" amplifying unit in a Tektronix 551 oscilloscope. The intensity of light received at the detector was displayed as a 120 cps signal in the oscilloscope. Phototube quality was maintained by preventing light from striking the cathode except during tests and by using neutral density filters to limit the total light intensity.

The mercury lamp was fixed to the support table; a focusing and slit system provided nearly parallel light at the nozzle. Monochromatic light was obtained through use of interference filters interposed in the beam. The phototube was supported on a protractor arm which rotated about the reservoir-nozzle assembly, enabling measurements of scattered light to be made at angles as high as 120° from the forward beam. The spectral source was positioned so the maximum beam intensity was found on a straight line connecting the source, center of the nozzle, and detector. Stray light was minimized by the positioning of opaque paper tubes along the light paths between the reservoir and the source and phototube assemblies. A glass duct 0.050 x 0.25 in. in cross section and 1 in. high (see Fig. 5) was fixed to the nozzles employed for extinction measurements. All surfaces of the duct except those in the direct optical path were darkened to prevent spurious reflections. A brass plate containing a pinhole (see Fig. 6) was attached to the nozzle employed for scattering measurements, and served to minimize the width of the beam incident on the particle-gas stream flowing from the single nozzle passage.

The distance from the nozzle face to the light beam was determined by vertical positioning of the reservoir. The maximum beam height possible with the reservoir in its support was 3 in. Measurements in this investigation were made at a distance of 0.375 above the nozzle.

Procedure

Size Measurements

Characterization of the size of particles after dispersion is complicated by the difficulties in obtaining a proper sample. The possible bias of the sample because of loss of very small or very large particles must be minimized. Samples were processed in three ways: "as received" material was dusted onto collodion-wetted microscope slides; de-agglomerated particles collected for light microscope analysis were obtained by placing collodion-wetted microscope slides in the particle-gas stream; and de-agglomerated particles collected for electron microscope analysis were obtained by diverting a portion of the gas-particle stream into a small tube leading to an exposed filter on which the particles were trapped.

Electron microscope examination employed a replica of the particles on the filter paper, prepared by the standard technique of vapor deposition of carbon over the sample. Magnification of samples ranged from 200 to 500 in the case of light microscope examination, and from 12,000 to 35,000 in the case of electron microscope examinations.

Extinction and Scattering Measurements

The purpose of the extinction measurements was to obtain values of the extinction parameter, b_e, which is defined as

$$b_e = \frac{1}{\rho_p x} \ln(I_0/I) \qquad (1)$$

where I_0 and I are the intensities of light impinging upon and passing through a particle-gas stream; ρ_p is the mass density of the particles in the gas volume; and x is the thickness of the carrier gas stream. The magnitudes of I_0 and I were displayed on an oscilloscope; linearity of the entire optical-electronic system was assured by calibration. The path length, x, was fixed at 0.25 in. (0.636 cm). The particle density, ρ_p, was dependent on both the particle and gas flow rates; consequently, both the particle and gas flow rates were determined. The particle flow rate was fixed by the weight of the charge placed in the cylinder of the feed mechanism and by the rate of cylinder motion. The gas flow rates were determined with a rotameter accurate to $\pm 1\%$ of scale reading. Typical values of the mass flow of gases through the nozzle in the absence of particle flow as a function of applied pressure are shown in Figs. 7 and 8. Also shown in these figures for comparison are the mass flow rates that would apply for choked flow for the same nozzle, assuming discharge coefficients of 0.64 for nitrogen and 0.61 for helium. Additional gas-flow measurements were performed with particles in the gas stream; for the particle concentrations employed (particle mass flow rates were less than approximately 0.1 times gas mass flow rates), no noticeable differences in the nozzle flow calibrations were observed.

Preparation for extinction measurements included (a) loading of the dust meter, (b) initiation of the mercury arc, (c) adjustment of the magnitude of the incident intensity signal, I_0, on the oscilloscope through the use of neutral density filters in the beam and a variable attenuator in the amplifier unit, (d) adjusting the reservoir height, (e) positioning the movable arm at 0°, and (f) starting the particle-gas streams.

The measurements made following the start of the particle-gas stream included the attenuated light intensity, I, the reservoir pressure, P_N, and the time elapsing until dust flow ceased. An alternative to the latter measurement was to measure both the loaded weight of particles and the compacted particle height; the known rate of cylinder advance (and consequently the known feed rate of particles) permitted interruption of the particle flow at will.

The procedure for scattering measurements was essentially the same as for extinction measurements; additional parameters recorded were the scattered intensity, I_s, and phototube displacement angle (i.e., scattering angle), θ.

Data Reduction

Extinction Measurements

The basic relationship between the extinction parameter and the intensities of light incident on and passing through the sample, the sample density, and the sample thickness is given by Eq. (1). The particle density may be specified, in the case of the two-phase flow system employed in these tests, from the appropriate gas density at the optical measuring station and the gas and particle mass flows.

The dependence of b_e on the light intensity ratio and particle mass density is shown in Fig. 9. These results were obtained using Eq. (1) and the experimental path length of 0.636 cm (0.25 in.). Typical experimental variables are listed in Table I.

Scattering Measurements

The total intensity of scattered light was found by integration of the curves of intensity against angle. This intensity was subtracted from the total intensity incident upon the sample to give the exit intensity which would prevail if only scattering losses occurred. For reference, the extinction parameter was also determined during the light scattering tests and was found to be essentially the same as that determined during tests with the extinction apparatus.

RESULTS OF EXPERIMENTAL INVESTIGATIONS

Size Measurements

Carbolac 1

The nominal particle radius of Carbolac 1 as quoted by the manufacturer is 0.0045 microns (Ref. 16). In electron micrographs of Carbolac 1 dispersed in a wetting liquid (Ref. 16), particles or particle agglomerates having radii from the primary size of 0.0045 microns to as large as 1 micron were shown. However, as a bulk powder, Carbolac 1 agglomerates may typically be orders of magnitude larger than the agglomerates dispersed in liquid media. In the experiments conducted under this program, large-radius agglomerates were observed in the "as received" samples, as illustrated in Fig. 10. Similar agglomerates were reduced in size by passage

through the dust meter and then through the dispersing nozzle. The resultant reduced size is shown in the photographs in Figs. 11 and 12. An examination of the particle stream farther from the nozzle shows a particle radius somewhat larger than that at the nozzle exit, in agreement with the arguments for agglomeration in the stream according to the calculation outlined in Appendix I.

Tungsten

The nominal radius of the tungsten powder employed in these tests was, according to the manufacturer's estimates, 0.01 microns (Refs. 11 and 13). In both Ref. 11 and 13, however, photographs of the powder show very large, loose aggregates having effective radii of the order of 1 micron or greater. This form is similar to that found during this investigation.

Photographs of the "as received" tungsten powder used in this study are shown in Figs. 13 and 14. As is evident in these figures, the radius of tungsten particle agglomerates before dispersion is quite large. The form of the tungsten after dispersion is shown in Fig. 15. It is evident from Fig. 15 that the radius of the dispersed tungsten was approximately the same as that of the dispersed Carbolac, although the nominal particle radius was approximately twice as large. The forces responsible for agglomeration of tungsten are probably smaller than is the case with Carbolac, however, principally because the tungsten surfaces are cleaner (Ref. 13).

Extinction Measurements

Carbolac 1

The extinction parameter, b_e , was determined for Carbolac 1 under a variety of conditions: the nozzle passage lengths employed were 0.25, 0.75 and 1.25 in.; applied gas supply pressures were varied from 20 to 45 psia; and two gases, nitrogen and helium, were employed as carriers. Typical results are plotted in Figs. 16 to 20. In Fig. 16, the increase in b_e with increasing reservoir pressure is shown at a single wavelength of 0.435 microns. In Figs. 17 to 19, the variation of extinction parameter with wavelength is shown for the two carrier gases at pressures of 25, 35 and 45 psia, respectively. Theoretical values of b_e for carbon particles having radii of 0.125 and 0.16 micron are shown on Figs. 16 to 19 for comparison. These theoretical results were taken from Ref. 7. The two radii of 0.125 and 0.16 microns were selected because (a) these sizes appear to be representative of those found in the particle stream, and (b) these sizes are sufficiently separated in magnitude that the theoretical effect of particle size on the extinction parameter can be discerned.

The maximum value of the extinction parameter measured experimentally was 58,000 cm^2/gm which was obtained at a wavelength of 0.25 microns. The following

conditions were employed for the particular test: passage diameter, 0.020 in., passage length, 1.25 in., reservoir pressure 45 psia, and helium carrier gas.

The effects of varying passage lengths and carrier gases are also shown in Figs. 16 to 19. For each carrier gas, the time during which the shear forces acted was proportional to the nozzle length. Thus, increased nozzle length should have resulted in a decreased average agglomerate size. Also, changing from nitrogen to helium gas resulted in a net velocity increase for fixed pressure supply conditions; this should also have assisted in decreasing average agglomerate size, since the amount of shear was increased in the restrictive flow nozzle. Experimentally, both increased nozzle length and the use of helium in place of nitrogen increased the measured extinction parameter.

As noted on Fig. 1, the maximum theoretical extinction parameter for a wavelength of 0.4 microns is 68,000 cm^2/gm and occurs for a particle radius of approximately 0.1 microns. It can also be seen from this figure that lower values of extinction parameter should theoretically be obtained for particles either larger or smaller than 0.1 microns. For instance, a particle having a radius of 0.0045 microns (the nominal radius for Carbolac 1 powder) has a theoretical extinction parameter of approximately 30,000 cm^2/gm. Similarly, a particle having a radius of 0.36 microns also has a theoretical extinction parameter of approximately 30,000 cm^2/gm. It is not surprising, therefore, that the maximum measured extinction parameter at this wavelength (58,000 cm^2/gm as shown on Fig. 19) is less than the maximum theoretical extinction parameter since particle agglomerates of many sizes exist in the gas stream according to the photographs in Fig. 12.

It is interesting to note that a shear configuration which would completely break up all particle agglomerates (so that only particles having radii of 0.0045 microns were present in the stream) would result in a theoretical extinction parameter approximately half of the measured value. Such a loss in extinction parameter could be avoided in a gaseous nuclear rocket by using particles having nominal diameters greater than the value for Carbolac 1. Since the particle radius for maximum extinction parameter is a function of wavelength (see Fig. 1), it would be desirable to employ a nominal particle size chosen on the basis of the wavelength which is responsible for the greatest wall heating in a gaseous nuclear rocket engine.

Experimental extinction data at a wavelength of 0.36 microns for Carbolac 1 are summarized in Fig. 20, in which the measured extinction parameters are plotted in terms of a de-agglomeration parameter, $\rho_g V^2 L_N/g$. The de-agglomeration parameter, expressed in cm-atm, represents approximately the product of the kinetic energy which can be dissipated by shear and the length over which this shear can act. A more complete correlation of the experimental results with the test parameters would require an extensive investigation of equilibrium particle size which would be obtained by matching shear forces to agglomerative forces, and a determination of the rate of approach to an equilibrium particle radius in very long passages.

Tungsten

The experimental conditions for the determination of the extinction parameter of tungsten were the same as those employed in the experiments with carbon. Typical results are plotted in Figs. 21-25. In Fig. 21 the effect of reservoir pressure on extinction parameter at a wavelength of 0.43 microns is shown. In Figs. 22-24 the variation of extinction parameter with wavelength is shown for reservoir pressures of 25, 35 and 45 psia, respectively.

The maximum extinction parameter measured for tungsten was 8200 cm^2/gm at a wavelength of 0.435 microns. Conditions prevailing during this measurement were: passage diameter, 0.020 in., passage length, 1.25 in., and reservoir pressure, 45 psia with helium as the carrier gas. The maximum theoretical extinction parameter of tungsten at 0.40 microns wavelength as shown in Fig. 2 is 20,000 cm^2/gm, corresponding to a particle radius of 0.07 microns. It can also be seen from Figs. 1 and 2 that a given fractional change in particle radius from the particle radius for maximum absorption parameter will result in a greater decrease in extinction parameter for tungsten particles than for carbon particles. For example, at a wavelength of 0.4 microns, the maximum extinction parameters and corresponding particle radii are 68,000 cm^2/gm at 0.1 microns and 20,000 cm^2/gm at 0.05 microns for carbon and tungsten, respectively. Halving or doubling the particle radius results in a reduction in b_e of approximately 35% for tungsten (from 20,000 cm^2/gm to 12,500 cm^2/gm) but only approximately 25 % for carbon (from 68,000 cm^2/gm to 50,000 cm^2/gm). Therefore, a given dimensionless distribution of particle size about the particle size for maximum extinction parameter would yield an extinction parameter equal to a smaller fraction of the theoretical maximum extinction parameter for tungsten particles than for carbon particles. In addition, because the wavelength for maximum extinction parameter for tungsten particles is less than that for graphite particles, a given large-size particle agglomerate would provide an extinction parameter which is a smaller fraction of the maximum theoretical value for tungsten than for graphite.

A summary of the extinction data for tungsten at a wavelength of 0.36 microns is shown in Fig. 25 in which the extinction parameter is plotted vs the deagglomeration parameter, $\rho_g V^2 L_N / g$. The general trend of the data is similar to that occurring for Carbolac, although the fraction of the theoretical maximum extinction parameter which is attained is smaller.

Scattering Measurements

Carbolac 1

The results of measurements of the angular dependence of the intensity of light scattered by carbon particles is shown in Fig. 26. Also shown are the incident light intensity and the attenuated light intensity measured as a function of

angle. These measurements were made at an incident light wavelength of 0.435 microns, for the nozzle geometry shown in Fig. 6 with a reservoir pressure of 40 psia, using helium as the carrier gas.

The energy removed from the beam by extinction and scattering was determined from the experimental curves. In the case of scattering, the curve of scattered intensity against angle was integrated, assuming symmetry of the scattered light about the forward beam. Approximately 30% of the total scattered light was found at angles greater than 6 deg. The experimental value of the scattering parameter of Carbolac 1 at a wavelength of 0.435 microns was 26,400 cm^2/gm. The measured value of the extinction parameter for this same experiment was 47,100 cm^2/gm (compared to 50,300 cm^2/gm for the same nozzle conditions but with the nozzle configuration shown in Fig. 5). The ratio of the extinction parameter to the scattering parameter is 1.78, which may be compared to a theoretical ratio of 2.03 for a single particle radius of 0.16 microns.

Tungsten

The scattering parameter of tungsten was determined under conditions similar to those prevailing during the carbon tests. The results are shown in Fig. 27. Approximately 25% of the total scattered light was found at angles beyond 6 deg. The scattering and extinction parameters under the test conditions were 3900 and 6750 cm^2/gm, respectively. The experimental b_e/b_s ratio at 0.43 microns was thus 1.73 and may be compared to theoretical ratios at 0.4 microns of 2.0 and 1.54 for particle radii of 0.05 and 0.14 microns, respectively.

REFERENCES

1. Weinstein, H. and R. Ragsdale: The Coaxial Flow Reactor - A Gaseous Nuclear Rocket Concept. ARS Preprint 1518-60, presented at the ARS 15th Annual Meeting, Washington, D. C., December 1960.

2. Barré, J. J.: Contribution to the Problem of the Nuclear Rocket Engine. Proceedings of the VIII International Astronautical Congress, Barcelona, 1957, Springer-Verlag, Berlin, 1958, pp. 1-14.

3. Krascella, N. L.: Theoretical Investigation of Spectral Opacities of Hydrogen and Nuclear Fuel. United Aircraft Corporation Research Laboratories Report RTD-TDR-63-1101, November 1963.

4. Krascella, N. L.: Tables of the Composition, Opacity and Thermodynamic Properties of Hydrogen at High Temperatures. United Aircraft Corporation Research Laboratories Report B910168-1, September 1963.

5. Marteney, P. J. and N. L. Krascella: Theoretical and Experimental Investigations of Spectral Opacities of Mixtures of Hydrogen and Diatomic Gases. United Aircraft Corporation Research Laboratories Report RTD-TDR-63-1102, November 1963.

6. Roback, R. W.: Thermodynamic Properties of Coolant Fluids and Particle Seeds for Gaseous Nuclear Rockets. United Aircraft Corporation Research Laboratories Report C-910092-3, September 1964. **NASA CR-212.**

7. Krascella, N. L.: Theretical Investigation of the Absorption and Scattering Characteristics of Small Particles. United Aircraft Corporation Research Laboratories Report C-910092-1, September 1964. **NASA CR-210.**

8. Lanzo, C. D. and R. G. Ragsdale: Experimental Determination of Spectral and Total Transmissivities of Clouds of Small Particles. NASA Technical Note D-1405, September 1962.

9. Lanzo, C. D. and R. G. Ragsdale: Heat Transfer to a Seeded Flowing Gas From an Arc Enclosed by a Quartz Tube. NASA Technical Memorandum X-52005, June 1964.

10. Furini, B. and V. W. Uhl: Agglomeration: Theories and Influencing Factors. Preprint 16, Technical Session No. 5, 54th Annual Meeting, American Institute of Chemical Engineers, New York, December 2-7, 1961.

11. Ripley, R. L. and N. Lamprey: Preparation and Properties of Ultrafine Tungsten Powder. Ultrafine Particles, ed. by W. E. Kuhn, H. Lamprey and C. Sheer. John Wiley and Sons, New York, 1963, pp. 262-270.

12. Quantinetz, M., et al: The Production of Submicron Metal Powders by Ball-Milling with Grinding Aids. Transactions of the Metallurgical Society of AIME, Vol. 221, No. 12, 1961, pp. 1105-1110.

13. Lamprey, H. and R. L. Ripley: Ultrafine Tungsten and Molybdenum Powders. Journal of the Electrochemical Society, Vol. 109, No. 6, 1962, pp. 713-716.

14. Loftman, K. A.: Coatings Incorporating Ultrafine Particles. Ultrafine Particles, ed. by W. Kuhn, H. Lamprey and C. Sheer, John Wiley and Sons, New York, 1963, pp. 530-544.

15. Wright, B. M.: A New Dust-Feed Mechanism. Journal of Scientific Instruments, Vol. 27, No. 1, 1950, pp. 12-13.

16. Anonymous: Cabot Carbon Blacks under the Electron Microscope, 2nd Ed. Cabot Corporation, Boston, November 1953.

17. Smoluchowski, M.: Zeitschrift fur Physikalische Chemie, Vol. 92, 1917, p. 129.

18. Devir, S.: On the Coagulation of Aerosols (Part I). Journal of Colloid Science, Vol. 18, No. 8, 1963, pp. 744-756.

LIST OF SYMBOLS

a_e	Extinction coefficient, cm^{-1}
A	Area, cm^2 or $in.^2$
A_c	Cunningham correction factor, dimensionless
b_a	Absorption parameter, $cm^2\ gm^{-1}$
b_e	Extinction parameter, $cm^2\ gm^{-1}$
b_s	Scattering parameter, $cm^2\ gm^{-1}$
C_D	Nozzle discharge coefficient, dimensionless
D_N	Diameter of passage, cm or in.
g	Gravitational acceleration, 981 cm sec^{-2}
I_o	Incident intensity of light, erg $cm^{-2}\ sec^{-1}$
I	Transmitted or scattered intensity of light, erg $cm^{-2}\ sec^{-1}$
k	Boltzmann constant, 1.38×10^{-16} erg deg K^{-1}
L_N	Length of passage, cm or in.
$\dot{M}_g$	Mass flow rate of gas, gm sec^{-1} or lb sec^{-1}
$\dot{M}_P$	Mass flow rate of particles, gm sec^{-1} or lb sec^{-1}
n_g	Gas number density, cm^{-3}
n_P	Particle number density, cm^{-3}
P	Pressure, psia
R_P	Radius of particle, microns
t	Time, sec
T	Temperature, deg K or deg R
V	Velocity, cm sec^{-1} or ft sec^{-1}
x	Path length in particle stream, cm or in.

θ	Displacement angle of detector or scattering angle, deg
ϕ	Mean free path of gas molecules, cm or Å
λ	Wavelength of light, microns
μ	Viscosity coefficient, dyne sec cm^{-2}
ρ_g	Mass density of gas gm cm^{-3}
ρ_P	Mass density of particles, gm cm^{-3}
σ	Collision diameter of gas molecules, cm or Å
$\tau_{1/2}$	Collision half-life, sec

Subscripts

a	Absorption
e	Extinction
g	Gas
N	Nozzle
o	Reference state
P	Particle
s	Scattering

APPENDIX I

CALCULATION OF THE RATE OF PARTICLE AGGLOMERATION AS A FUNCTION OF INITIAL PARTICLE RADIUS

The theoretical derivation to define the rate of agglomeration of dispersed gas-particle systems was first presented in Ref. 17 and recently confirmed in Ref. 18. The equation for the rate of agglomeration by collision is:

$$-\frac{dn_p}{dt} = \frac{4}{3}\frac{\pi kT}{\mu}\left(1+\frac{A_c\phi}{R_p}\right)n_p^2 \qquad \text{(I-1)}$$

in terms of n_p = particle density, cm^{-3}

k = Boltzmann constant, 1.38×10^{-15} erg deg K^{-1}

T = temperature, deg K

μ = coefficient of viscosity, dyne sec cm^{-2}

A_c = Cunningham correction factor, 0.86

ϕ = mean free path of gas molecules, cm

R_p = particle radius, cm

t = time, sec

Integration of Eq. (I-1) yields the following expression relating the number of particles of the original size R_p at time t to the number existing at time $t = 0$:

$$\frac{1}{n_{p(t)}} - \frac{1}{n_{p(0)}} = \frac{4}{3}\frac{\pi kT}{\mu}\left(1+\frac{0.86\phi}{R_p}\right)t \qquad \text{(I-2)}$$

The mean free path of the gas molecules, ϕ, is given by:

$$\phi = \frac{0.707}{\pi n_g \sigma^2} \qquad \text{(I-3)}$$

where σ = collision diameter of gas molecules and n_g = number density of gas molecules. (For air at 1 atm and 293 K, σ = 3.71 Å and ϕ = 650 Å.) During the present investigation, a series of calculations were carried out using Eq. (I-2) to estimate the times required to effect significant particle agglomeration. The criterion used to define the agglomeration times was the collision half-life which is the time required for one half of the original number of particles to suffer collision with at least one other particle. By substitution of the numerical values for constant terms into Eq. (I-2) the collision half-life can be written as

$$\tau_{1/2} = \frac{0.75\,\mu}{(1.38 \times 10^{-16})\, n_0 T \left(1 + \frac{0.86}{R}\right)} \qquad \text{(I-4)}$$

The dependence of $t_{1/2}$ on initial particle size was calculated for the cases of 0.1 to 5.0 percent by mass carbon particles in nitrogen at 300 K and 1 atm, with the results plotted in Fig. 28. The collision half-life varies (for the case of 1 percent carbon) from 10^{-3} sec at approximately 1.5 x 10^{-2} microns radius to 1000 sec at approximately 6.5 microns radius.

The results shown in Fig. 28 should be taken as order of magnitude results because of the approximate nature of the model assumed in Ref. 18 and the requirement for the following assumptions:

1. The system consists of a monodispersion. The presence of a non-singular particle size has been cited as a reason for departure of agglomeration rates from the theoretical values, but the effect is not firmly established.

2. All collisions lead to agglomeration. The efficiency of collision has been found to be nearly unity; departure from theory because of inefficient collisions is of much less importance than the other factors above.

3. Molecular forces of the van der Waals type determine whether or not particles adhere once they collide, but do not influence the collision rate. This is well supported by experiment. The reasoning is that the average particle separation is too great for the van der Waals forces to play any part; thus particle collisional behavior entirely determines the coagulation rate.

4. The wall effect is neglected. The result of losses to the wall is a net particle density decrease with no sensible change in particle size; particles once joined to the walls remain.

5. The effect of electrical charge of particles on the rate is neglected. This effect is still the object of considerable study; the practical consideration is that the effect is important only in highly-charged

systems such as atmospheric clouds, and that the average charge on non-cloud particles is sufficiently low to warrant neglect of this factor in determination of the rate.

TABLE I

REPRESENTATIVE EXPERIMENTAL PARAMETERS AND RESULTS

Conditions: Passage Diameter, d_N - 0.020 in.
Passage Length, L_N - 0.75 in.
Reservoir Pressure, P_N - 35 psia
Wavelength, λ - 0.435 microns

Carrier Gas/ Particles	Gas Mass Flow Rate, $\dot{M}_g$-gm/sec	Gas Density, ρ_g-g/cm^3	Particle Mass Flow Rate $\dot{M}_P$-gm/sec	Particle Density, ρ_P-gm/cm^3	Mass Flow Ratio, M_P / M_g	Light Intensity Ratio, I_o / I	Extinction Parameter b_e-cm^2/gm	Extinction Coefficient a_e-cm^{-1}
Nitrogen/ Carbolac 1	0.440	1.14×10^{-3}	3.17×10^{-2}	8.23×10^{-5}	7.2×10^{-2}	8.35	40,700	3.34
Helium/ Carbolac 1	0.166	1.62×10^{-4}	1.66×10^{-2}	1.62×10^{-5}	1.0×10^{-1}	1.64	48,100	0.78
Nitrogen/ Tungsten	0.440	1.14×10^{-3}	2.70×10^{-2}	7.00×10^{-5}	6.1×10^{-2}	1.28	5,570	0.39
Helium/ Tungsten	0.166	1.62×10^{-4}	1.87×10^{-2}	1.83×10^{-5}	1.1×10^{-1}	1.07	5,780	0.10

THEORETICAL EFFECT OF PARTICLE RADIUS ON THE EXTINCTION AND ABSORPTION PARAMETERS OF SPHERICAL CARBON PARTICLES

DATA FROM REF. 7

TEMPERATURE, T = 2250 K

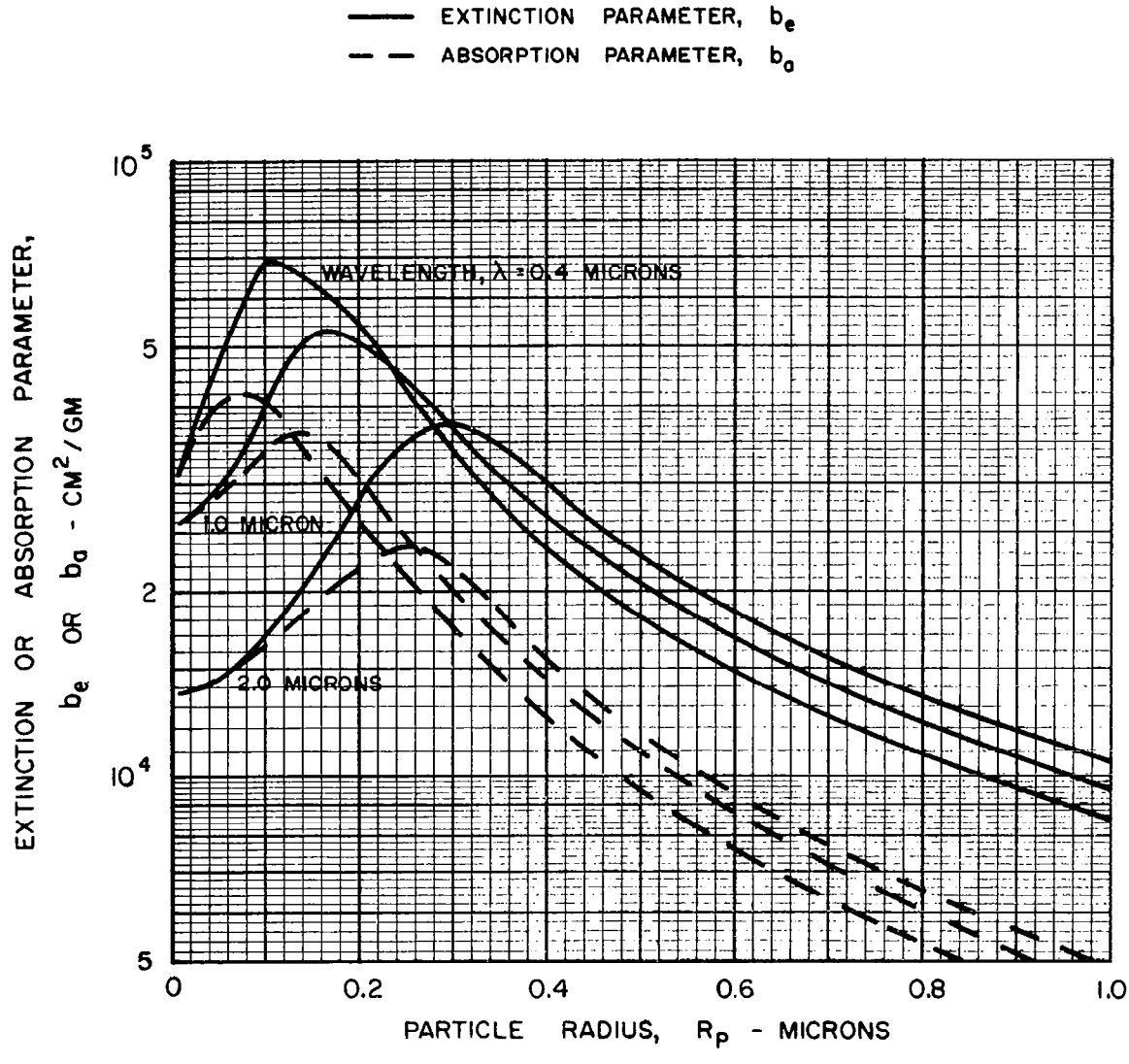

Figure 1

THEORETICAL EFFECT OF PARTICLE RADIUS ON THE EXTINCTION AND ABSORTION PARAMETERS OF SPHERICAL TUNGSTEN PARTICLES

DATA FROM REF. 7

TEMPERATURE, T = 298 K

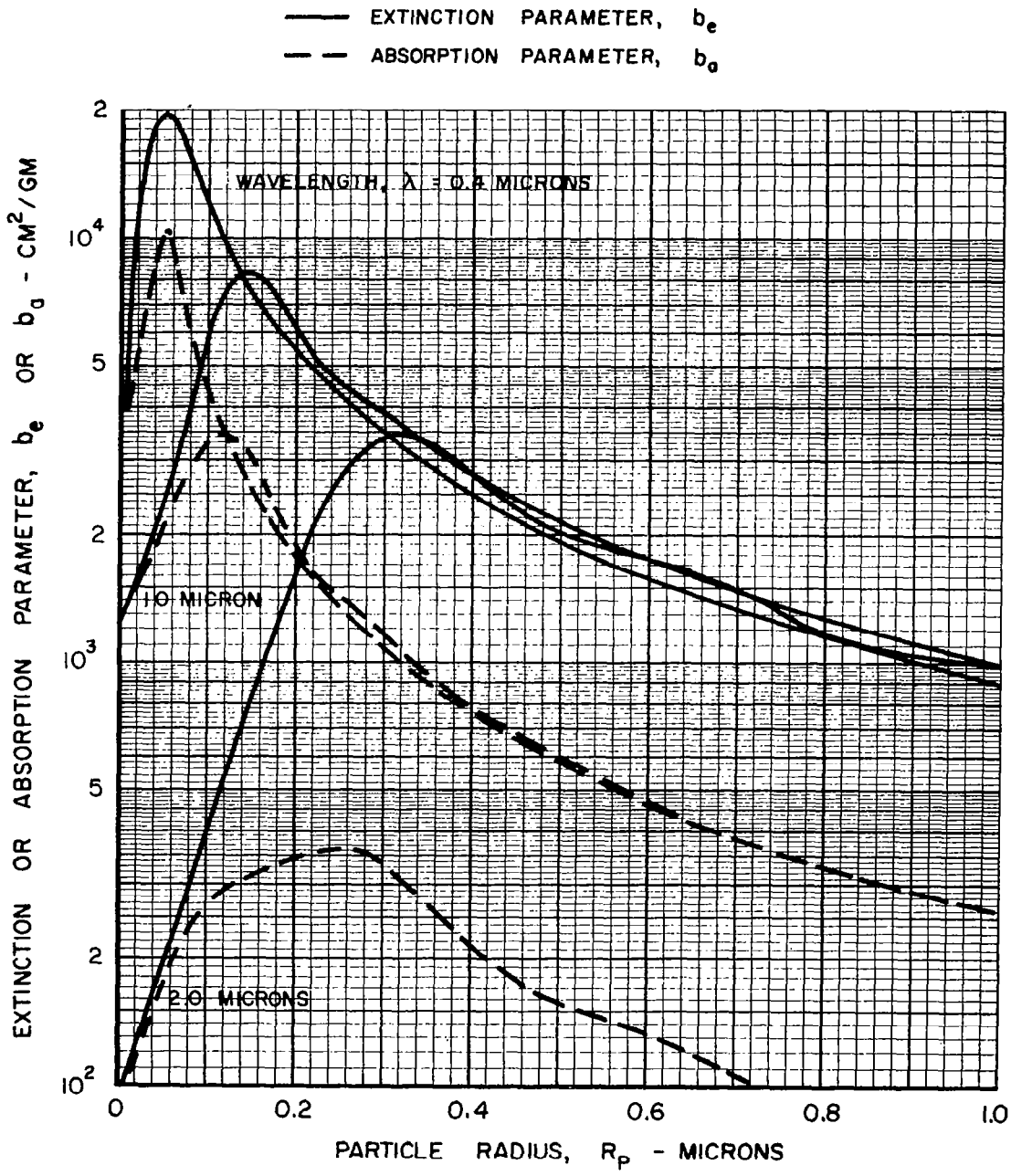

Figure 2

SCHEMATIC DIAGRAMS OF PARTICLE DISPERSER WITH ACCESSORY TEST EQUIPMENT

TOP VIEW

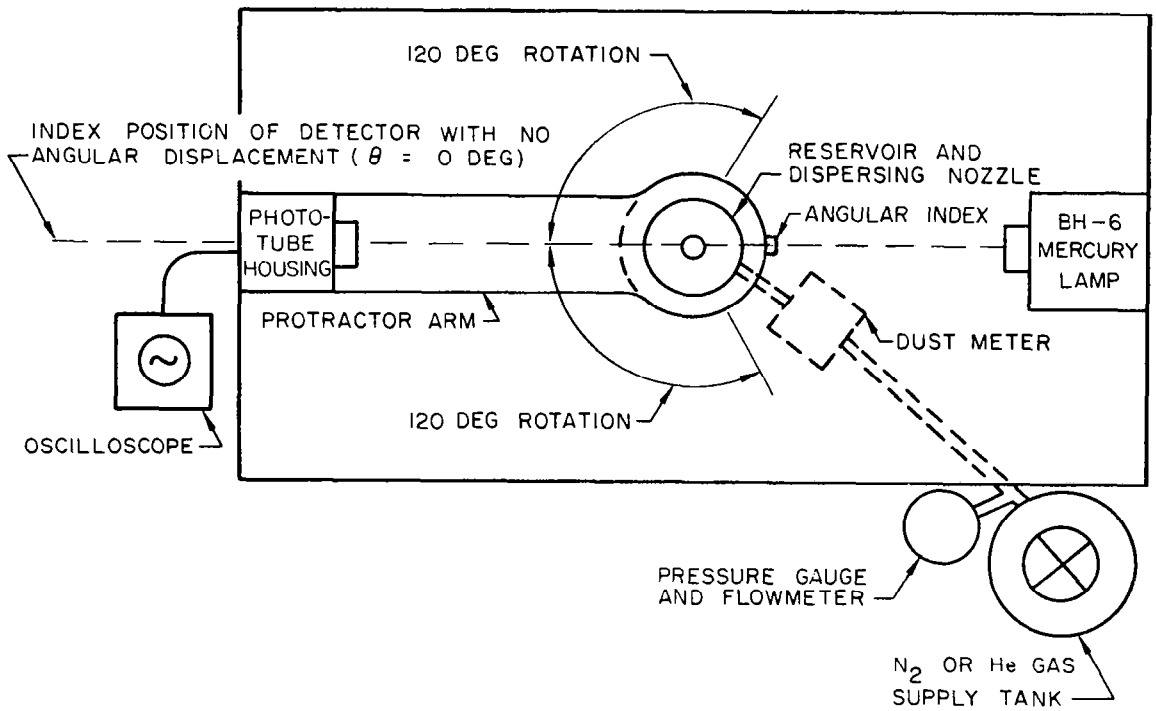

SIDE VIEW

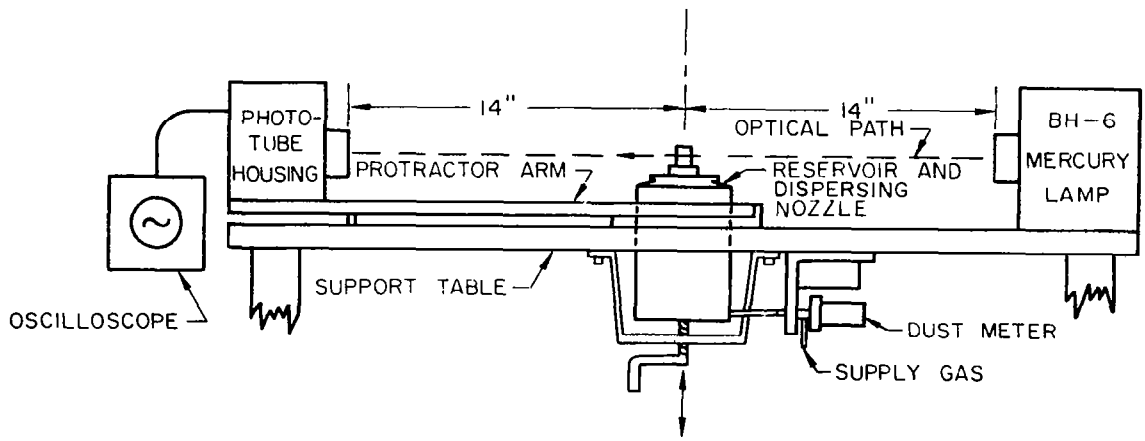

Figure 3

SECTIONAL VIEW OF PARTICLE RESERVOIR AND DISPERSING NOZZLE ASSEMBLY

ALL DIMENSIONS GIVEN IN INCHES

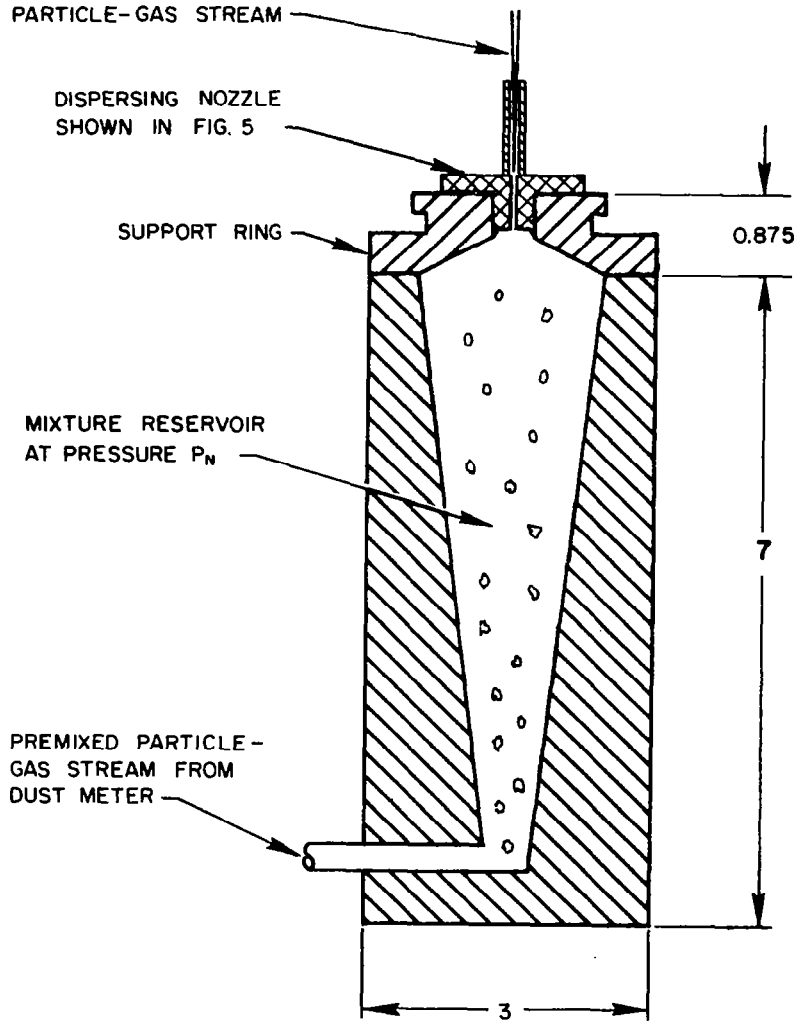

Figure 4

DISPERSING NOZZLE ASSEMBLY USED FOR EXTINCTION MEASUREMENTS

NOZZLE MATERIAL – COLD ROLLED STEEL
VIEWING DUCT MATERIAL – GLASS
ALL DIMENSIONS GIVEN IN INCHES

TOP VIEW

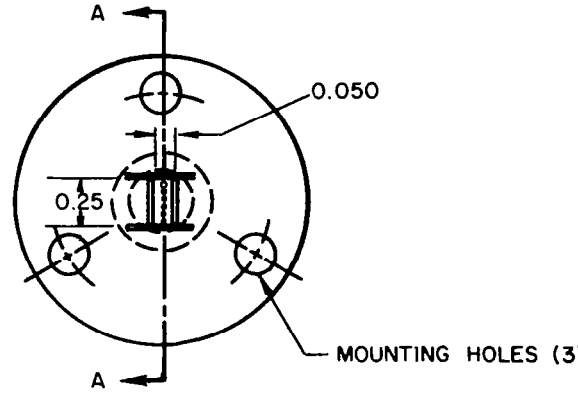

SIDE SECTIONAL VIEW AT A–A

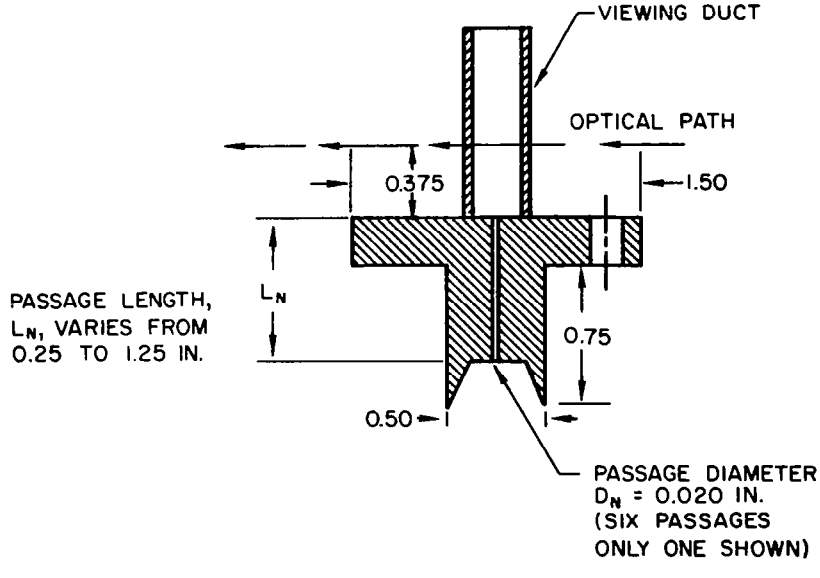

Figure 5

DISPERSING NOZZLE ASSEMBLY USED FOR SCATTERING MEASUREMENTS

NOZZLE MATERIAL – COLD ROLLED STEEL
PINHOLE PLATE MATERIAL – BRASS SHEET
ALL DIMENSIONS GIVEN IN INCHES

TOP VIEW

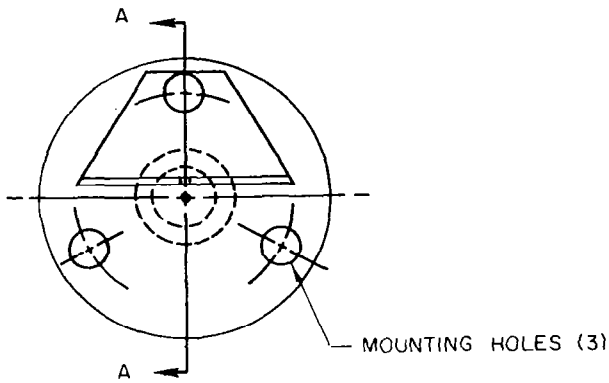

SIDE SECTIONAL VIEW AT A-A

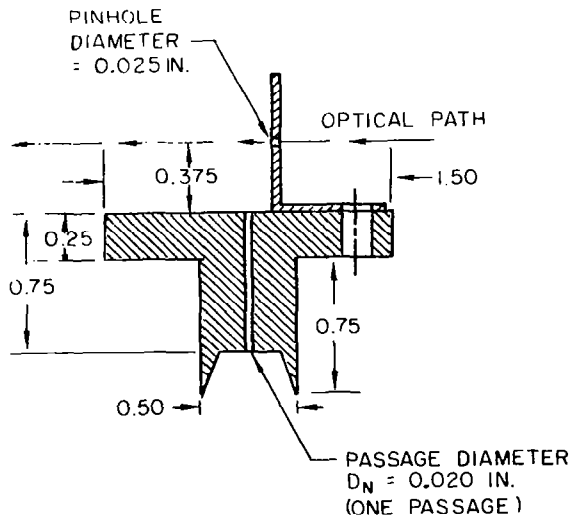

Figure 6

EFFECT OF RESERVOIR PRESSURE ON THE HELIUM MASS FLOW RATE THROUGH PARTICLE DISPERSING NOZZLE

RESERVOIR AND NOZZLE ASSEMBLY SHOWN IN FIG. 4

NOZZLE CONFIGURATION: SIX PASSAGES
PASSAGE DIAMETER, D_N = 0.020 IN.
PASSAGE LENGTH, L_N = 0.75 IN.

THEORETICAL FLOWS CALCULATED USING FOLLOWING RELATION
FOR CHOKED FLOW: $\dot{M}_{He} = 98.6\ P_N A_N C_D / \sqrt{T}$ GM / SEC

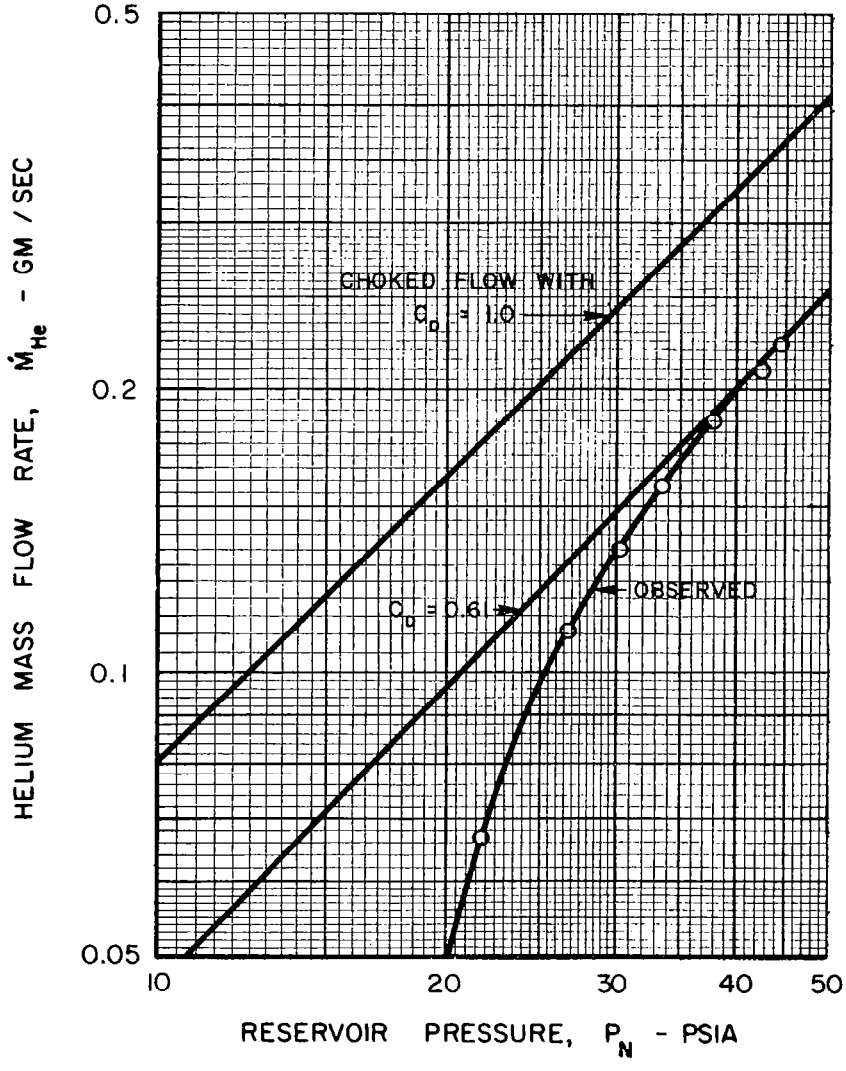

Figure 7

EFFECT OF RESERVOIR PRESSURE ON THE NITROGEN MASS FLOW RATE THROUGH PARTICLE DISPERSING NOZZLE

RESERVOIR AND NOZZLE ASSEMBLY SHOWN IN FIG. 4

NOZZLE CONFIGURATION: SIX PASSAGES
PASSAGE DIAMETER, D_N = 0.020 IN.
PASSAGE LENGTH, L_N = 0.75 IN.

THEORETICAL FLOWS CALCULATED USING FOLLOWING RELATION FOR CHOKED FLOW: $\dot{M}_{N_2} = 240\ P_N\ A_N\ C_D / \sqrt{T}$ GM / SEC

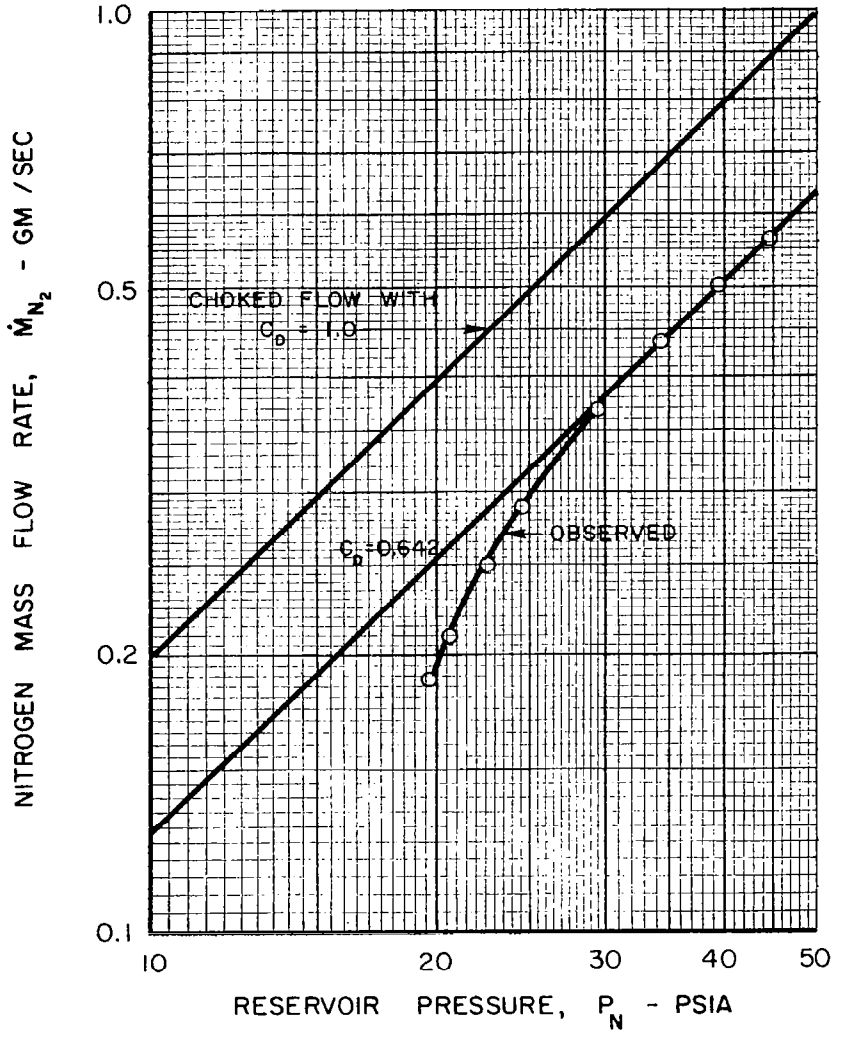

Figure 8

EFFECT OF THE RATIO OF INCIDENT TO ATTENUATED LIGHT INTENSITY ON THE EXTINCTION PARAMETER OF DISPERSED PARTICLES

$$b_e = \frac{1}{x} \ln\left(\frac{I_0}{I}\right) \frac{1}{\rho_P} \text{ CM}^2/\text{GM}$$

x = OPTICAL PATH LENGTH = 0.636 CM

ρ_P = PARTICLE MASS DENSITY, GM/CM^3

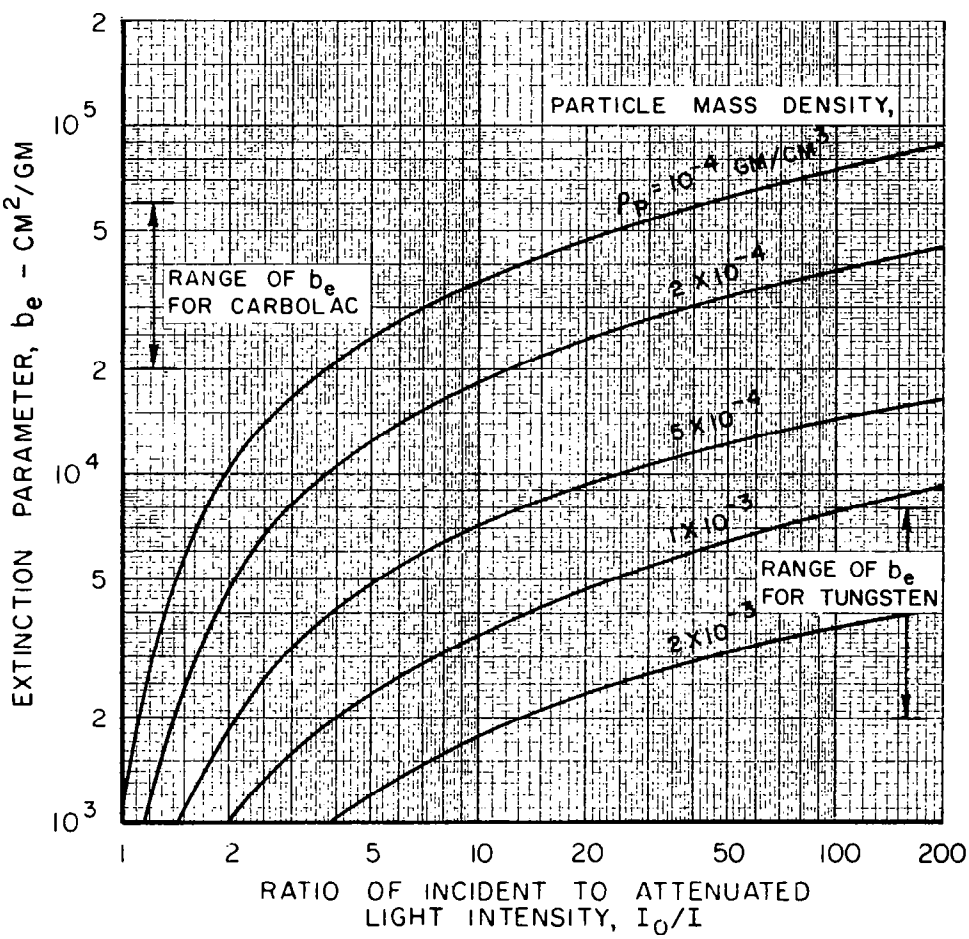

Figure 9

PHOTOGRAPHS OF CARBOLAC POWDER AT MAGNIFICATION OF 200

NOMINAL PARTICLE RADIUS, R_P - 0.0045 MICRONS

A) POWDER DUSTED ONTO MICROSCOPE SLIDE

B) POWDER COLLECTED FROM OUTLET OF DUST METER AT HELIUM PRESSURE OF 25 PSIA (PARTICLES SUBJECT ONLY TO IMPACT)

C) POWDER COLLECTED ON MICROSCOPE SLIDE AT HEIGHT OF ONE INCH ABOVE NOZZLE (PARTICLES SUBJECT TO BOTH IMPACT AND SHEAR)

HELIUM CARRIER GAS

RESERVOIR PRESSURE, P_N - 40 PSIA

PASSAGE DIAMETER, D_N - 0.020 IN.

PASSAGE LENGTH, L_N - 1.25 IN.

A)

50 MICRONS

B)

C)

Figure 10

ELECTRON MICROGRAPH OF DISPERSED CARBOLAC POWDER AT MAGNIFICATION OF 13,300

NOMINAL PARTICLE RADIUS, R_P - 0.0045 MICRONS

SAMPLE COLLECTED BY ASPIRATION THROUGH FILTER PAPER AT HEIGHT OF 1 IN. ABOVE NOZZLE

HELIUM CARRIER GAS
RESERVOIR PRESSURE, P_N - 40 PSIA
PASSAGE DIAMETER, D_N - 0.020 IN.
PASSAGE LENGTH, L_N - 1.25 IN.

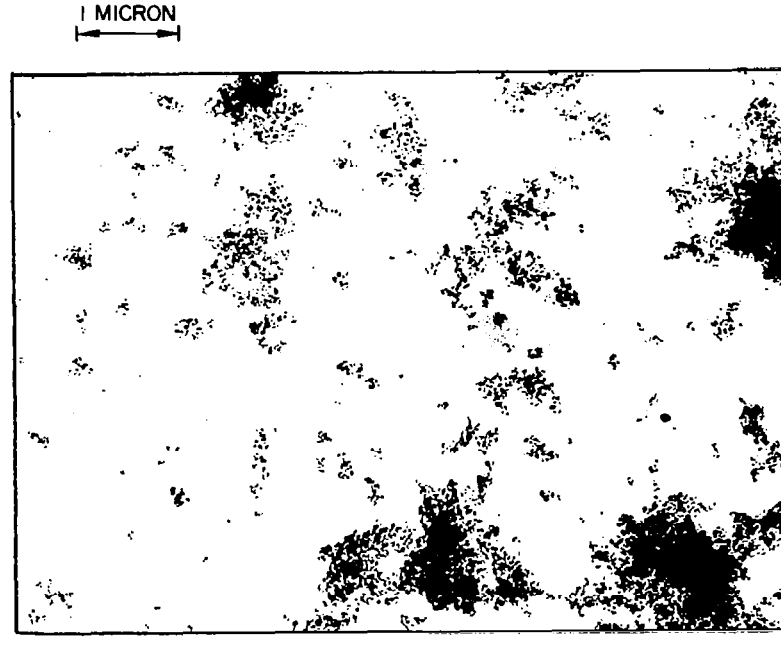

Figure 11

ELECTRON MICROGRAPH OF DISPERSED CARBOLAC POWDER AT MAGNIFICATION OF 21,000

NOMINAL PARTICLE RADIUS, R_P – 0.0045 MICRONS

SAMPLE COLLECTED BY ASPIRATION THROUGH FILTER PAPER AT HEIGHT OF 36 IN. ABOVE NOZZLE

HELIUM CARRIER GAS
RESERVOIR PRESSURE, P_N – 40 PSIA
PASSAGE DIAMETER, D_N – 0.020 IN.
PASSAGE LENGTH, L_N – 1.25 IN.

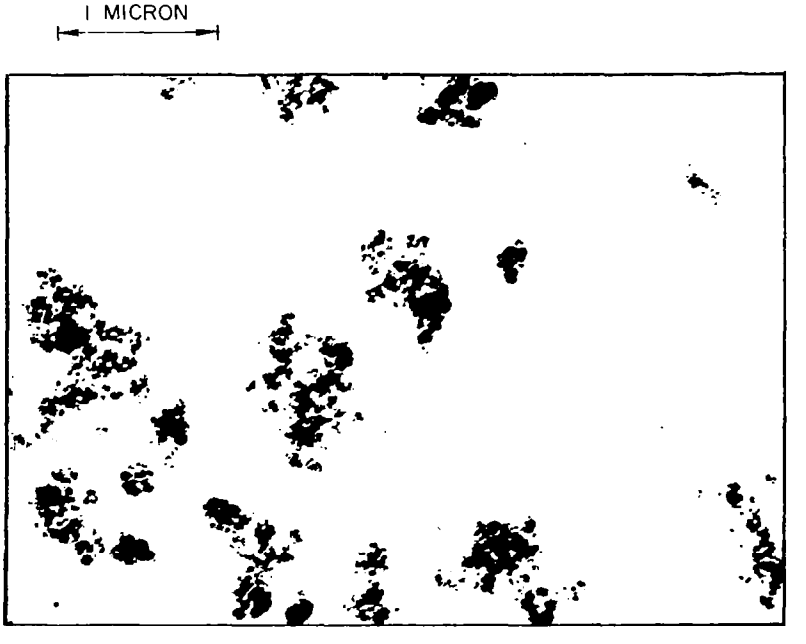

Figure 12

PHOTOGRAPH OF TUNGSTEN POWDER AT MAGNIFICATION OF 500

NOMINAL PARTICLE RADIUS, R_p – 0.01 MICRONS

POWDER DUSTED ONTO MICROSCOPE SLIDE

20 MICRONS

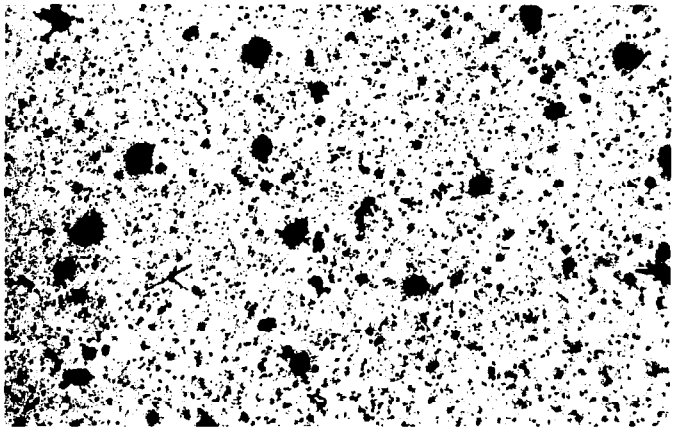

Figure 13

ELECTRON MICROGRAPH OF TUNGSTEN AT MAGNIFICATION OF 12,480

NOMINAL PARTICLE RADIUS, R_p - 0.01 MICRONS

POWDER DUSTED ONTO MICROSCOPE SLIDE

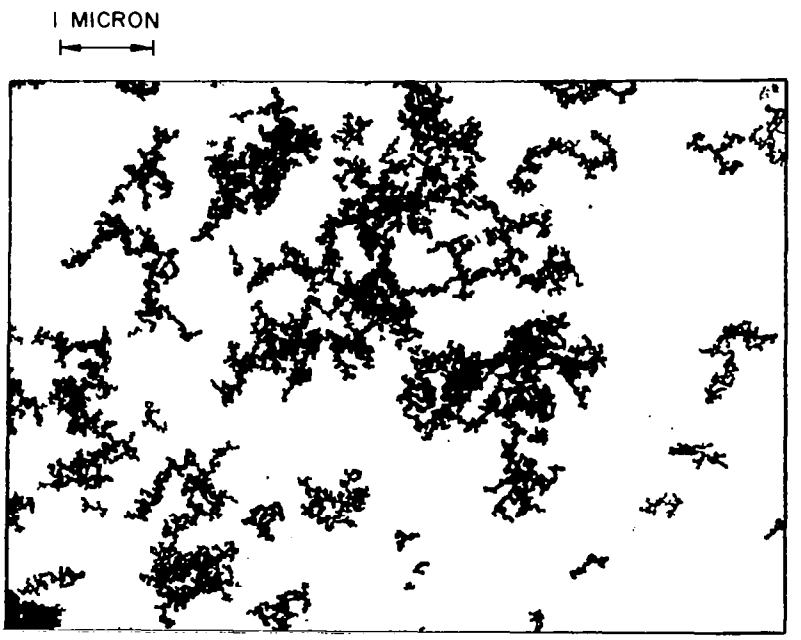

Figure 14

ELECTRON MICROGRAPH OF DISPERSED TUNGSTEN POWDER AT MAGNIFICATION OF 35,000

NOMINAL PARTICLE RADIUS, R_p – 0.01 MICRONS

SAMPLE COLLECTED BY ASPIRATION THROUGH FILTER PAPER AT HEIGHT OF 1 IN. ABOVE NOZZLE

HELIUM CARRIER GAS
RESERVOIR PRESSURE, P_N - 40 PSIA
PASSAGE DIAMETER, D_N – 0.020 IN.
PASSAGE LENGTH, L_N - 1.25 IN.

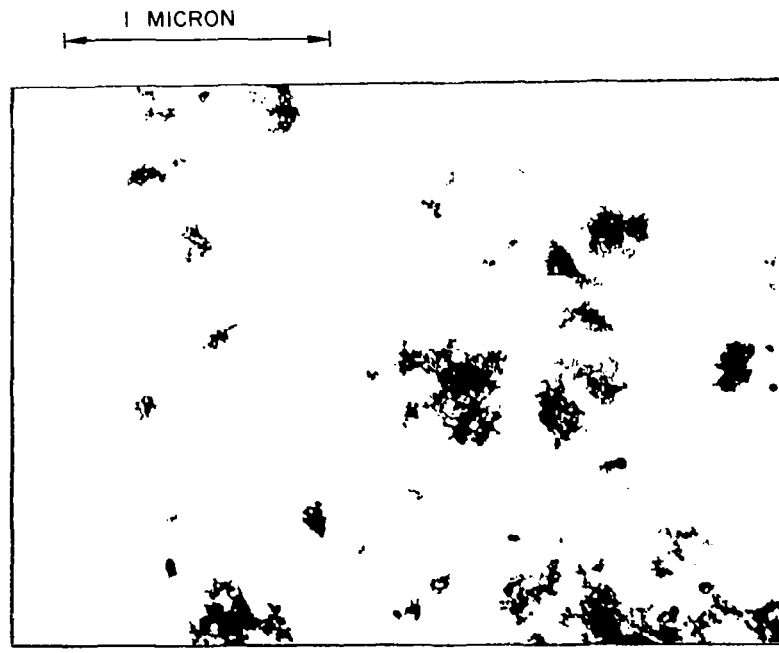

Figure 15

EFFECT OF RESERVOIR PRESSURE ON THE EXTINCTION PARAMETER OF DISPERSED CARBOLAC POWDER AT A WAVELENGTH OF 0.435 MICRONS

NOMINAL PARTICLE RADIUS, R_p = 0.0045 MICRONS
PASSAGE DIAMETER, D_N = 0.020 IN.
O - HELIUM CARRIER GAS
Δ - NITROGEN CARRIER GAS

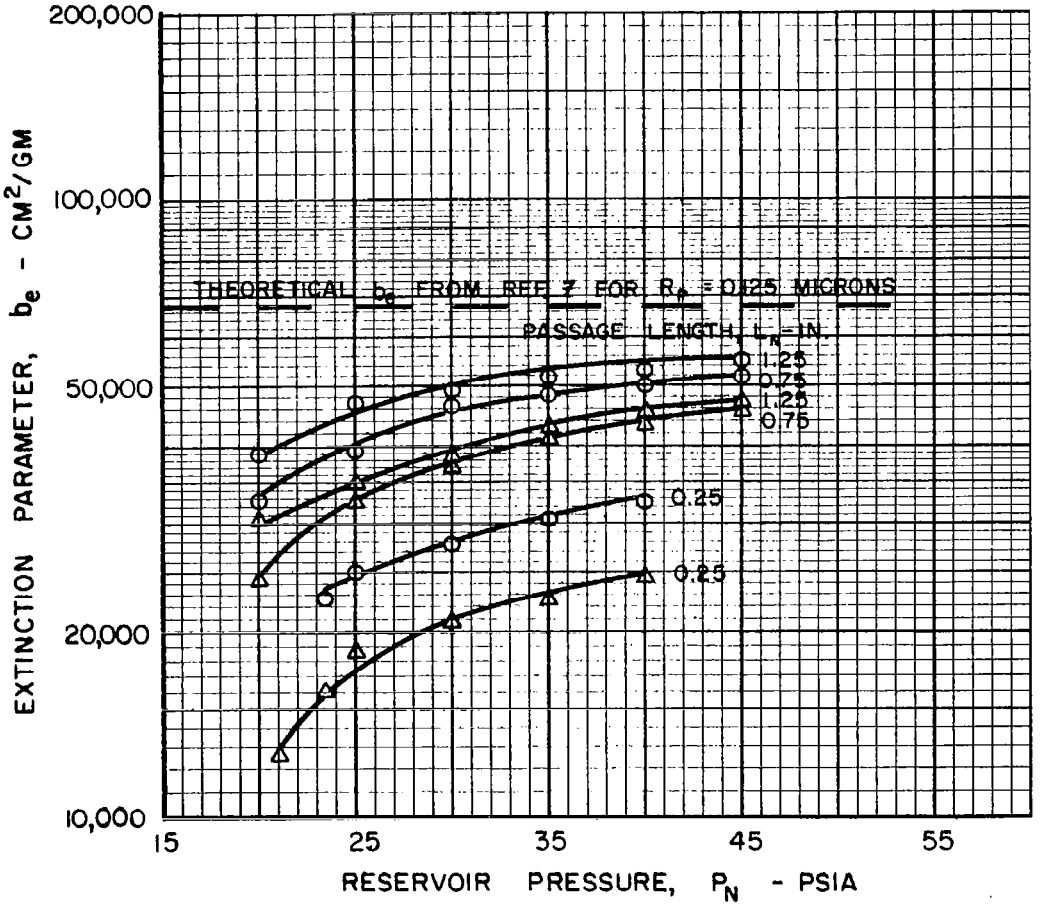

Figure 16

VARIATION OF THE EXTINCTION PARAMETER OF DISPERSED CARBOLAC POWDER WITH WAVELENGTH FOR SEVERAL CARRIER GASES AND PASSAGE LENGTHS AT A RESERVOIR PRESSURE OF 25 PSIA

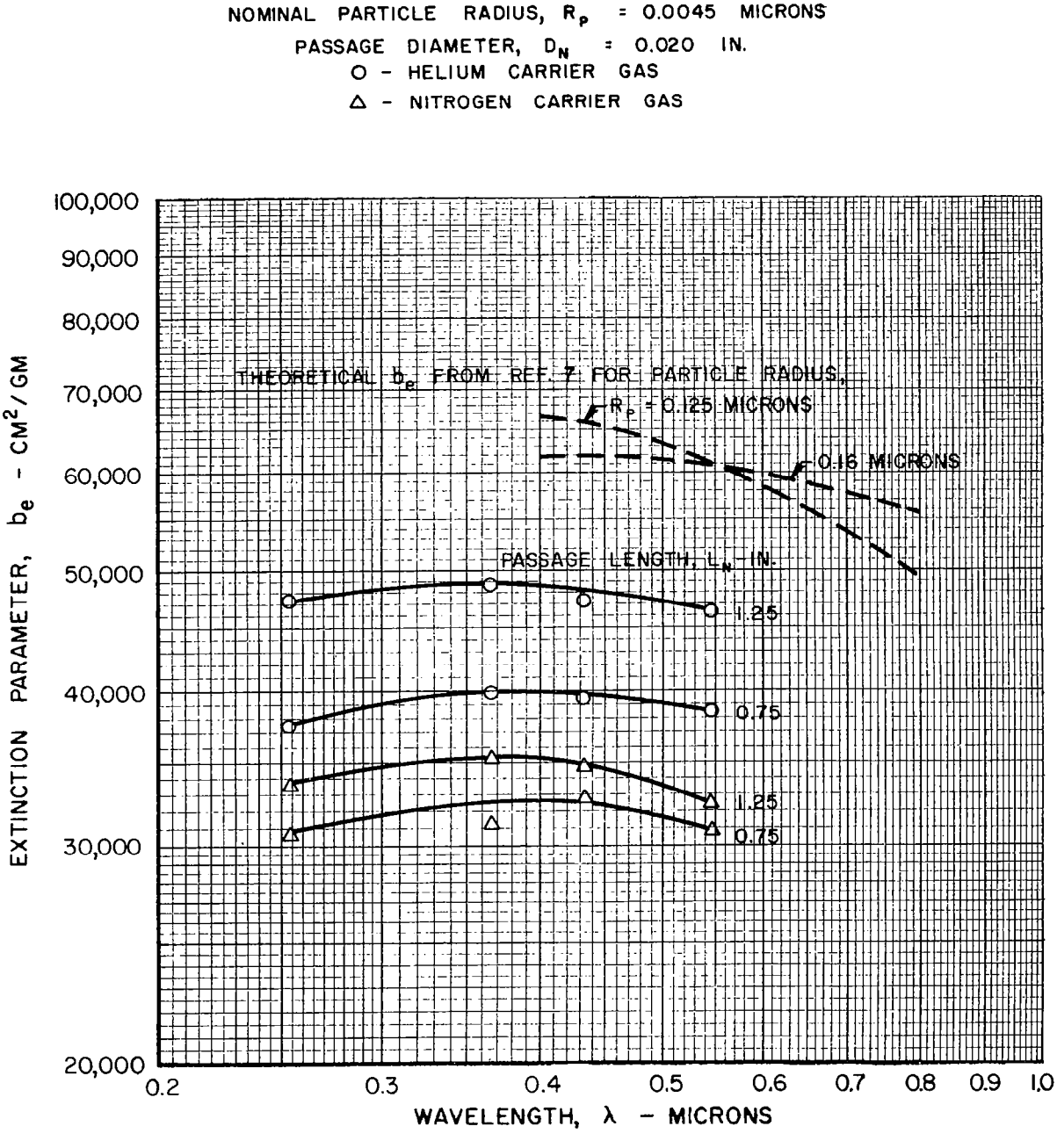

Figure 17

VARIATION OF THE EXTINCTION PARAMETER OF DISPERSED CARBOLAC POWDER WITH WAVELENGTH FOR SEVERAL CARRIER GASES AND PASSAGE LENGTHS AT A RESERVOIR PRESSURE OF 35 PSIA

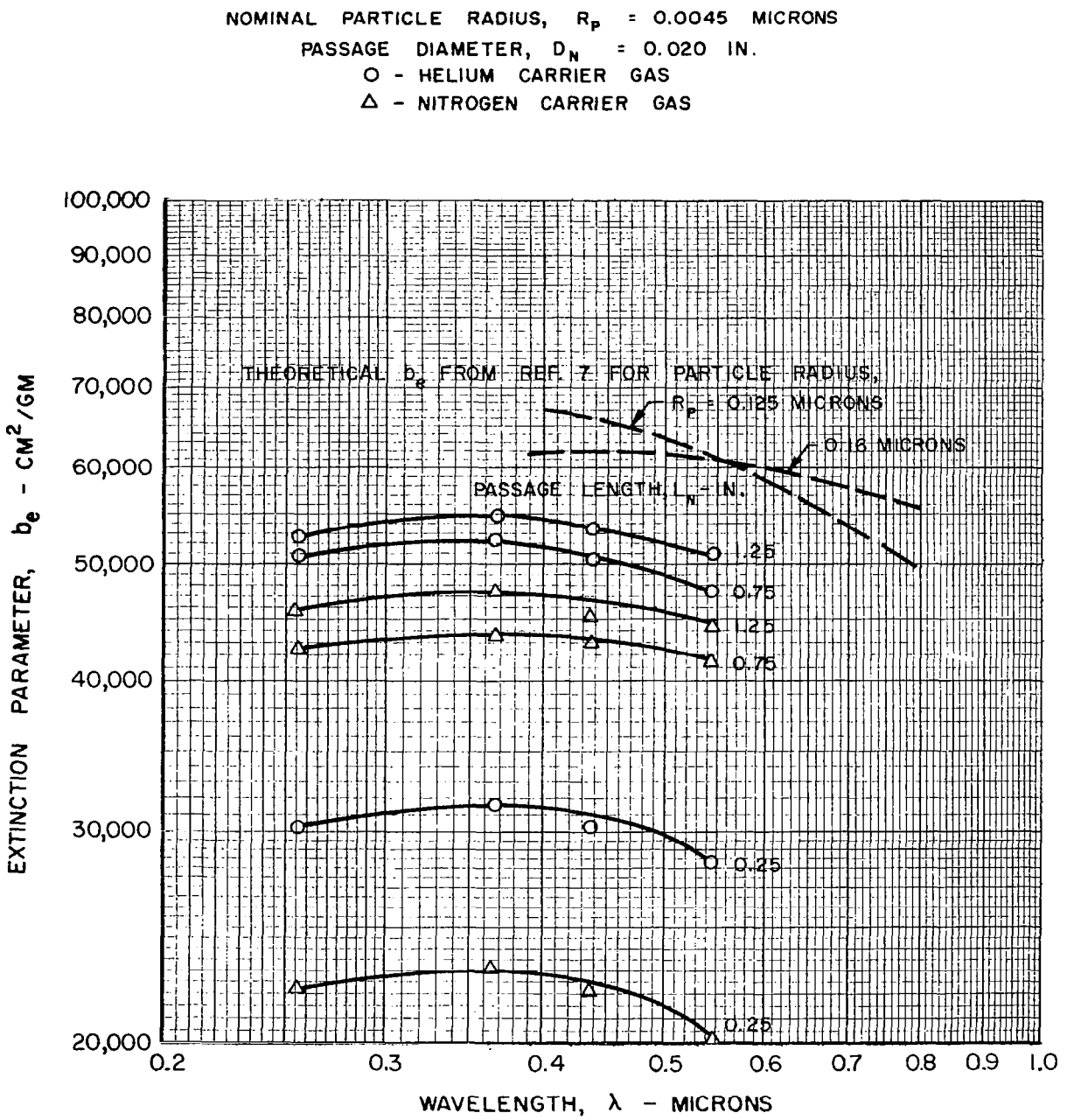

Figure 18

VARIATION OF THE EXTINCTION PARAMETER OF DISPERSED CARBOLAC POWDER WITH WAVELENGTH FOR SEVERAL CARRIER GASES AND PASSAGE LENGTHS AT A RESERVOIR PRESSURE OF 45 PSIA

NOMINAL PARTICLE RADIUS, R_p = 0.0045 MICRONS
PASSAGE DIAMETER, D_N = 0.020 IN.
○ - HELIUM CARRIER GAS
△ - NITROGEN CARRIER GAS

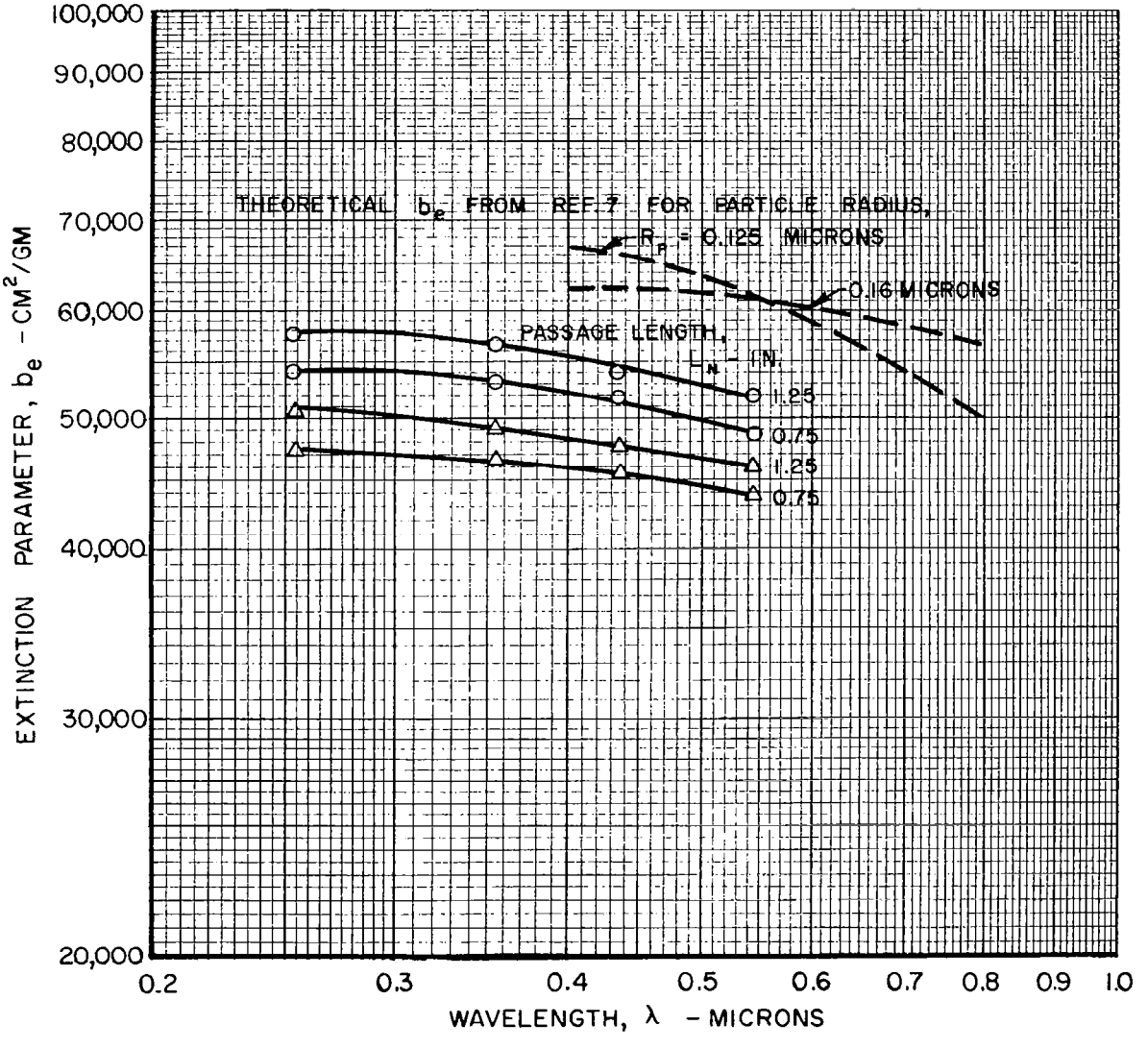

Figure 19

EFFECT OF THE DE-AGGLOMERATION PARAMETER ON THE MEASURED EXTINCTION PARAMETER OF CARBOLAC AT A WAVELENGTH OF 0.36 MICRONS

SYMBOL	CARRIER GAS	PASSAGE LENGTH	
		IN.	CM
O	HELIUM	0.25	0.636
D		0.75	1.91
◁		1.25	3.18
△	NITROGEN	0.25	0.636
◁		0.75	1.91
◺		1.25	3.18

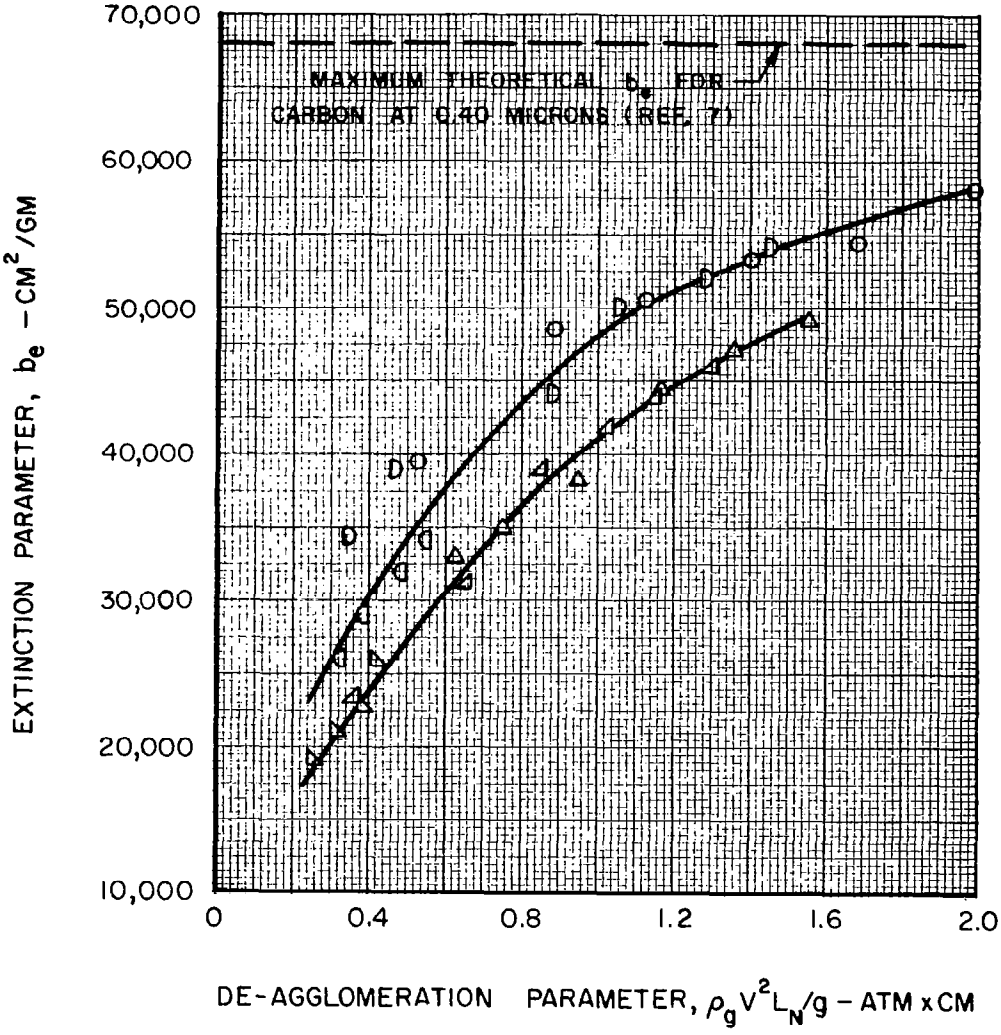

Figure 20

EFFECT OF RESERVOIR PRESSURE ON THE EXTINCTION PARAMETER OF DISPERSED TUNGSTEN POWDER AT A WAVELENGTH OF 0.435 MICRONS

NOMINAL PARTICLE RADIUS, R_P = 0.01 MICRONS
PASSAGE DIAMETER, D_N = 0.020 IN.
O - HELIUM CARRIER GAS
Δ - NITROGEN CARRIER GAS

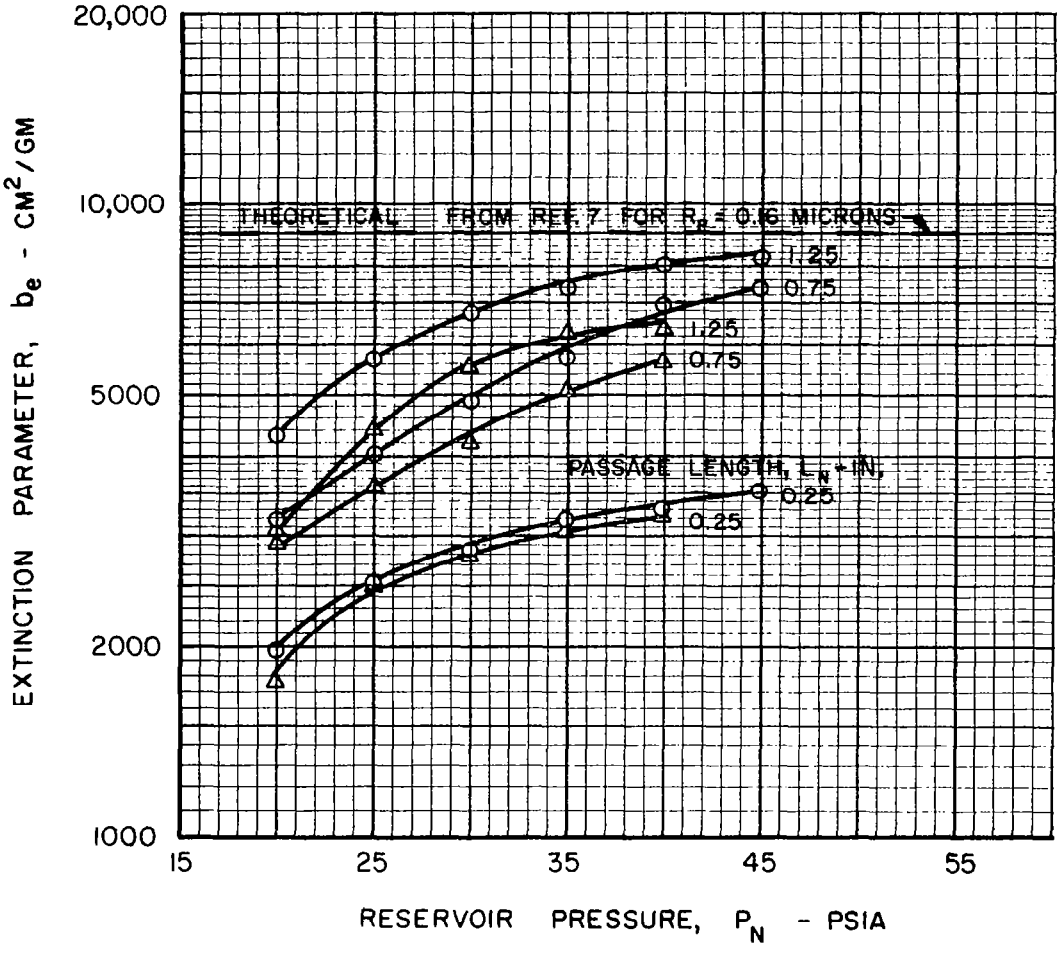

Figure 21

VARIATION OF THE EXTINCTION PARAMETER OF DISPERSED TUNGSTEN POWDER WITH WAVELENGTH FOR SEVERAL CARRIER GASES AND PASSAGE LENGTHS AT A RESERVOIR PRESSURE OF 25 PSIA

NOMINAL PARTICLE RADIUS, R_p = 0.01 MICRONS
PASSAGE DIAMETER, D_N = 0.020 IN.
O - HELIUM CARRIER GAS
Δ - NITROGEN CARRIER GAS

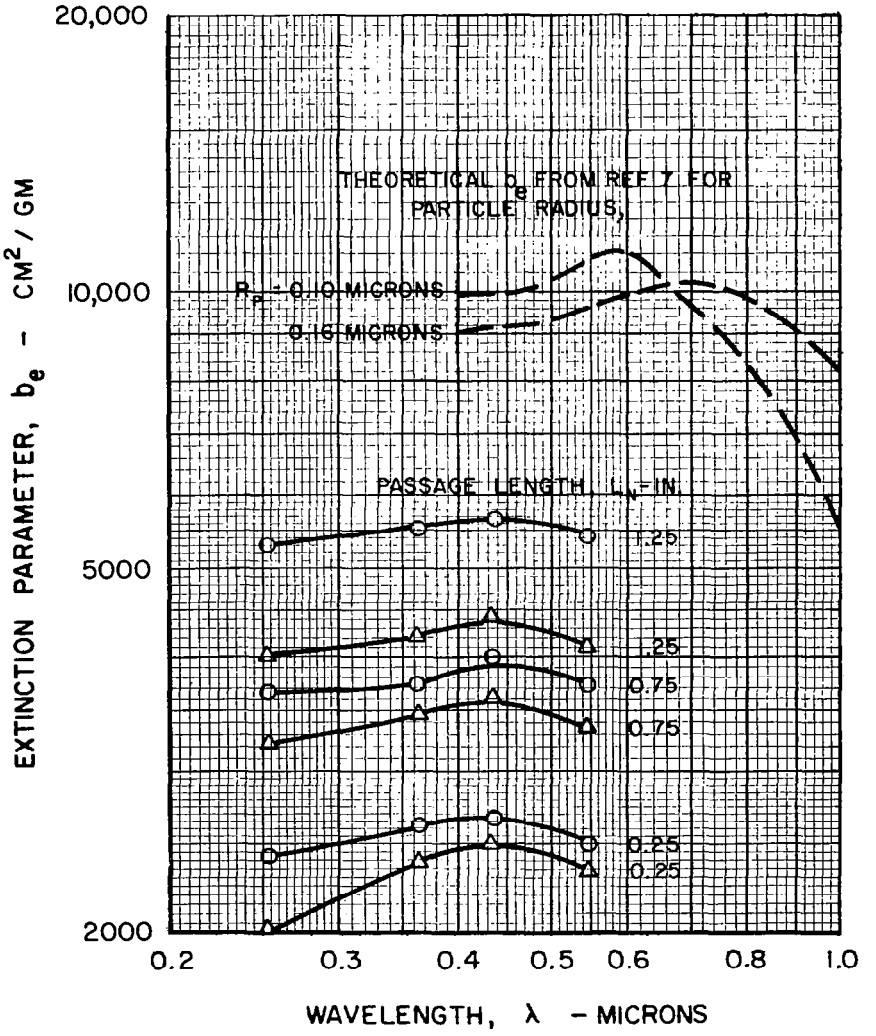

Figure 22

VARIATION OF THE EXTINCTION PARAMETER OF DISPERSED TUNGSTEN POWDER WITH WAVELENGTH FOR SEVERAL CARRIER GASES AND PASSAGE LENGTHS AT A RESERVOIR PRESSURE OF 35 PSIA

NOMINAL PARTICLE RADIUS, R_p = 0.01 MICRONS
PASSAGE DIAMETER, D_N = 0.020 IN.
O - HELIUM CARRIER GAS
Δ - NITROGEN CARRIER GAS

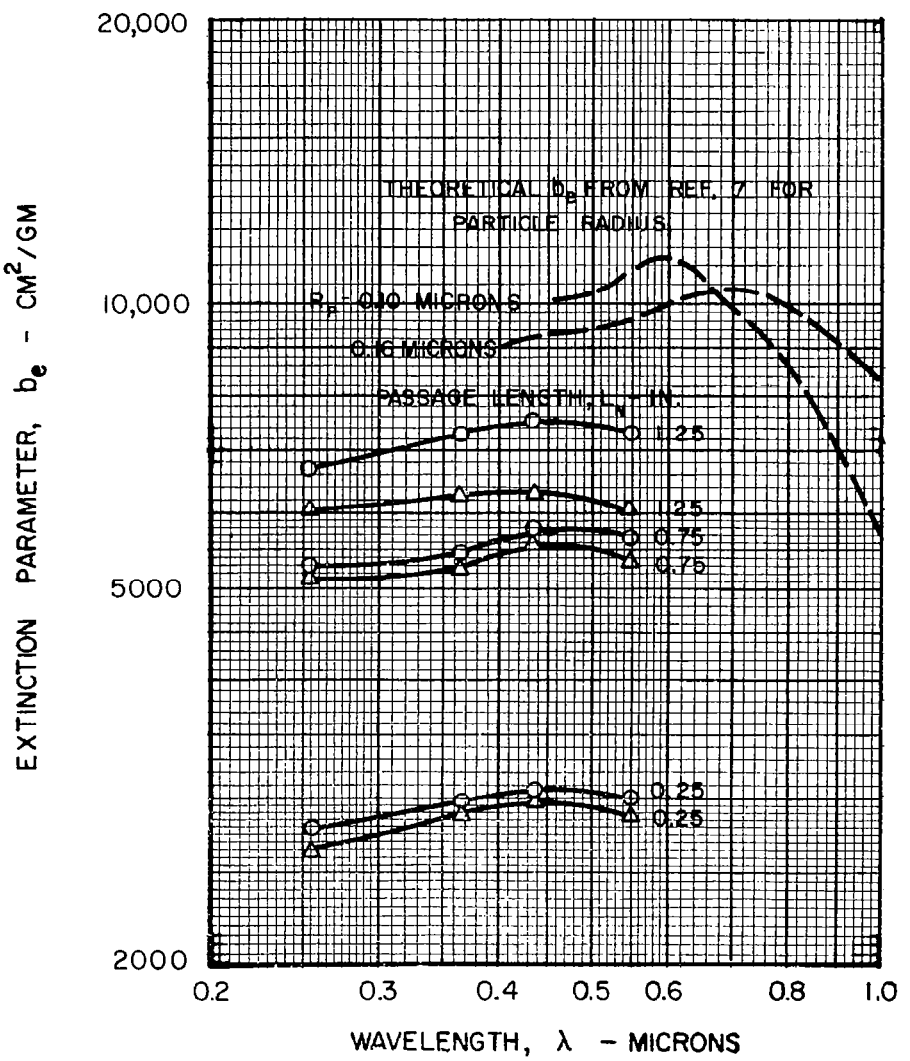

Figure 23

VARIATION OF THE EXTINCTION PARAMETER OF DISPERSED TUNGSTEN POWDER WITH WAVELENGTH FOR SEVERAL CARRIER GASES AND PASSAGE LENGTHS AT A RESERVOIR PRESSURE OF 45 PSIA

NOMINAL PARTICLE RADIUS, R_p = 0.01 MICRONS
PASSAGE DIAMETER, D_N = 0.020 IN.
○ - HELIUM CARRIER GAS
△ - NITROGEN CARRIER GAS

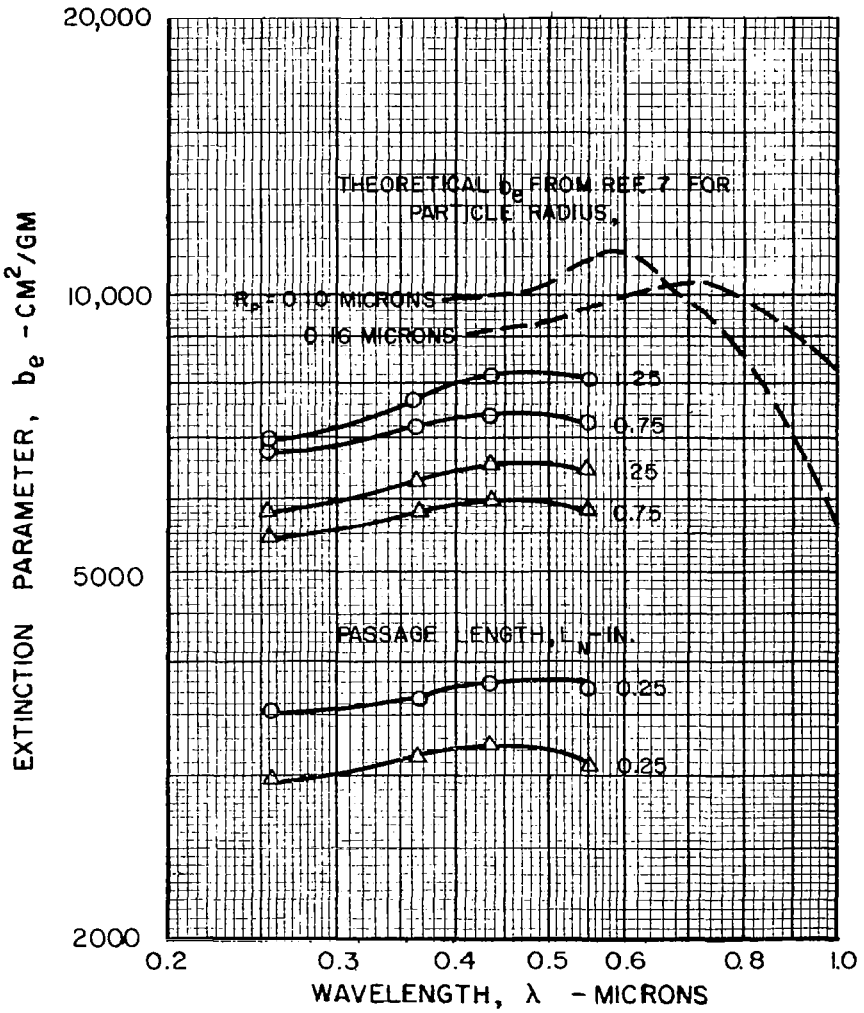

Figure 24

EFFECT OF THE DE-AGGLOMERATION PARAMETER ON THE MEASURED EXTINCTION PARAMETER OF TUNGSTEN AT A WAVELENGTH OF 0.36 MICRONS

SYMBOL	CARRIER GAS	PASSAGE LENGTH	
		IN.	CM
O	HELIUM	0.25	0.636
D		0.75	1.91
◻		1.25	3.18
Δ	NITROGEN	0.25	0.636
◿		0.75	1.91
◺		1.25	3.18

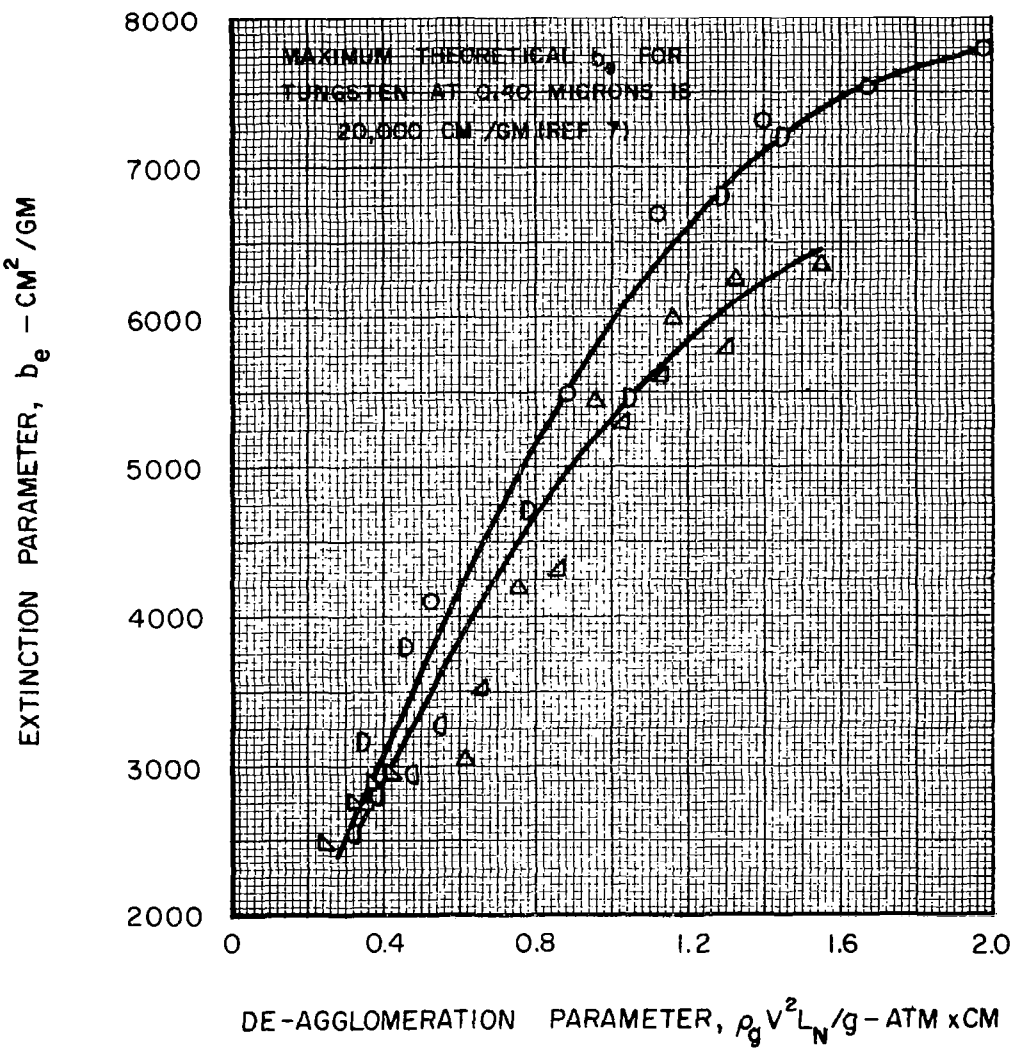

Figure 25

VARIATION OF THE INTENSITY OF LIGHT TRANSMITTED AND SCATTERED BY TUNGSTEN POWDER AS A FUNCTION OF ANGULAR DISPLACEMENT OF DETECTOR

HELIUM CARRIER GAS
RESERVOIR PRESSURE, P_N = 40 PSIA
PASSAGE DIAMETER, D_N = 0.020 IN.
PASSAGE LENGTH, L_N = 0.75 IN.
WAVELENGTH, λ = 0.435 MICRONS

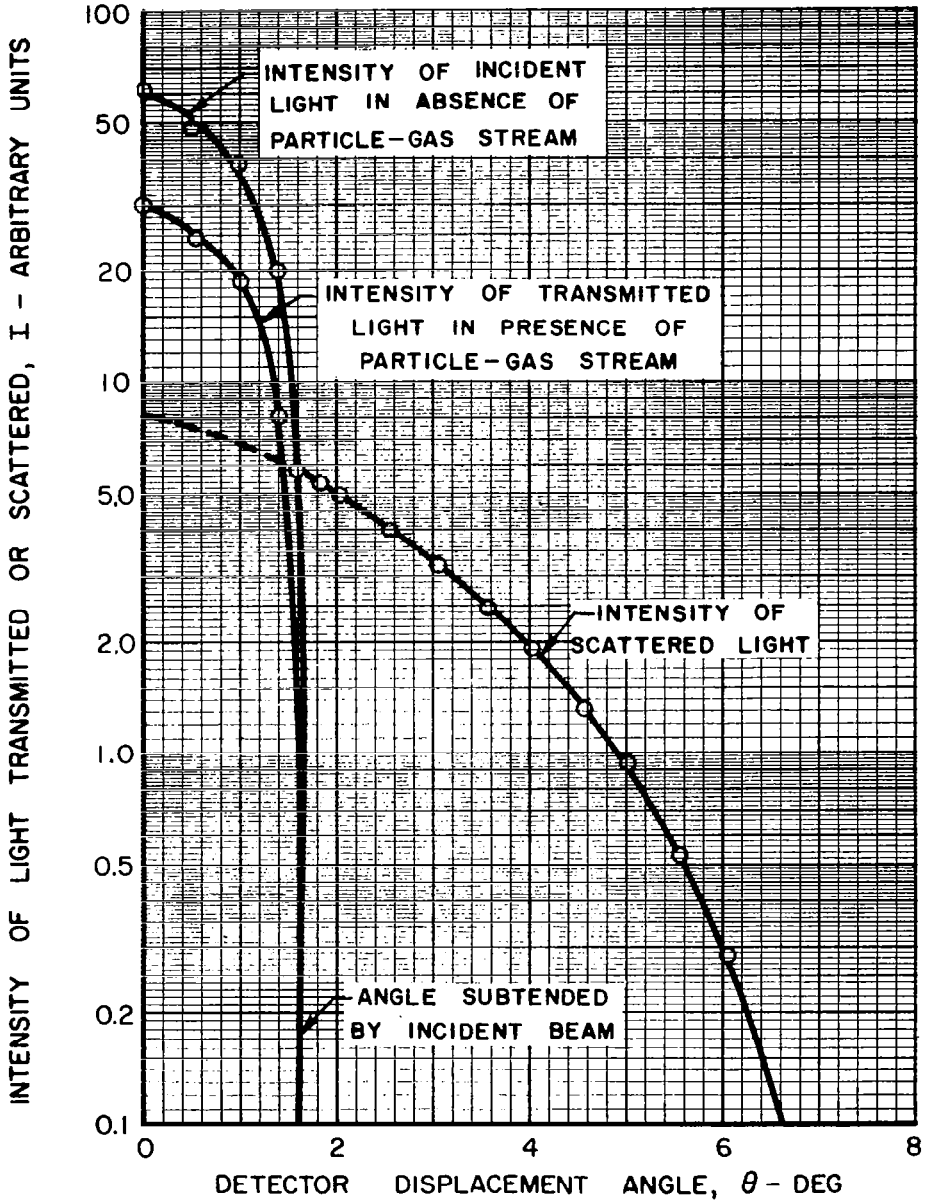

Figure 26

VARIATION OF THE INTENSITY OF LIGHT TRANSMITTED AND SCATTERED BY CARBOLAC POWDER AS A FUNCTION OF ANGULAR DISPLACEMENT OF DETECTOR

HELIUM CARRIER GAS
RESERVOIR PRESSURE, P_N = 40 PSIA
PASSAGE DIAMETER, D_N = 0.020 IN.
PASSAGE LENGTH, L_N = 0.75 IN.
WAVELENGTH, λ = 0.435 MICRONS

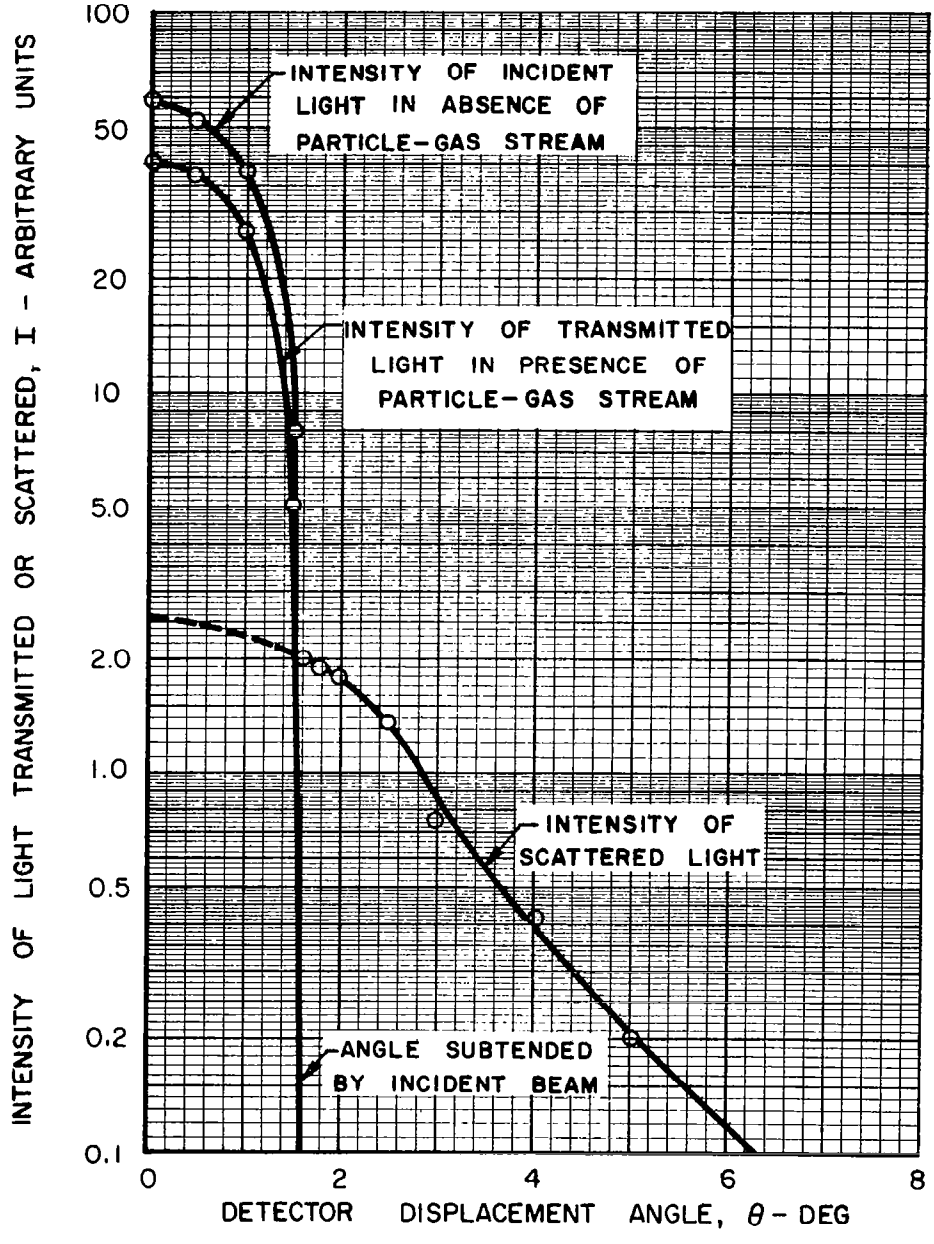

Figure 27

THEORETICAL EFFECT OF INITIAL PARTICLE RADIUS ON THE TIME REQUIRED FOR COLLISION - INDUCED AGGLOMERATION OF 50 PERCENT OF INITIAL PARTICLES (COLLISION HALF - LIFE)